

Supporting Information

Efficient Photocatalytic C-3 Thiocyanation of Indoles over Tetraphenylsilane-Based Porous Aromatic Frameworks

Yuxuan He ^a, Linzhu Cao ^a, He Wang ^a, Fengchao Cui ^{*a}, and Xin Tao ^{*a}

^a Key Laboratory of Polyoxometalate and Reticular Material Chemistry of Ministry Education,
Faculty of Chemistry, Northeast Normal University, Changchun, 130024, China

*E-mail: cuifc705@nenu.edu.cn; taox091@nenu.edu.cn

Table of Contents

1. Materials and Characterization.....	3
1.1 Materials	3
1.2 Instrumentations.....	3
1.3 Electrochemical measurements	4
2. Synthesis of TEPS-4Br and TEPS-PAFs	4
2.1 Synthesis of tetrakis(4-bromophenyl) silane (TEPS-4Br).....	4
2.2 Synthesis of PAF-403³.....	5
2.3 Synthesis of PAF-404³.....	6
2.4 Synthesis of PAF-405³.....	6
3. Typical procedure for photocatalytic C-3 thivialocyanation of indoles.....	7
4. Recycling experiment.....	7
5. Computational details.....	7
6. PXRD patterns	8
7. N₂ adsorption/desorption isotherms.....	8
8. Pore size distribution	9
9. TGA curves.....	9
10. SEM images	10
11. TEM image	10
12. TEM elemental mapping.....	10
13. XPS spectra.....	11
14. Tauc plots.....	12
15. VB-XPS spectra.....	12
16. PL spectra	13
17. Time-resolved fluorescence spectra.....	13
18. Supplementary tables	14
19. Scavenger experiments	16
20. Recyclability of PAF-405.....	17
NMR data	18
NMR spectra.....	21
References.....	37

1. Materials and Characterization

1.1 Materials

Unless otherwise noted, all materials were used as received from commercial sources without further purification. tris(4-ethynylphenyl)amine, 1,3,5-tris(4-ethynylphenyl)benzene and 2,4,6-tris(4-ethynylphenyl)-1,3,5-triazine were purchased from Innochem Chemicals. Anhydrous Et₃N and anhydrous DMF, *n*-butyllithium and 1,4-dibromobenzene were purchased from Energy Chemicals. Anhydrous MgSO₄ was purchased from Sinopharm Chemical. Methanol, acetone, HCl, dichloromethane and tetrahydrofuran were purchased from Titan.

1.2 Instrumentations

The ¹H NMR and ¹³C NMR spectra were obtained in dimethyl sulfoxide on Varian Inova 500 MHz spectrometer. ¹³C cross-polarization magic angle-spinning (CP-MAS) solid-state NMR spectra were obtained using a Bruker Avance III model 400 MHz NMR spectrometer at a MAS rate of 5 kHz. Fourier transforms infrared (FT-IR) analysis was performed on the Nicolet IS50 FTIR spectrometer. The powder X-ray diffraction (PXRD) measurements were carried out on the Rigaku SmartLab X-ray diffractometer with Cu-K α radiation. Thermal gravimetric analysis (TGA) was measured on the METTLER-TOLEDO TGA/DSC 3+ analyzer at the 10 °C min⁻¹ in N₂ atmosphere from room temperature to 800 °C. The N₂ adsorption-desorption isotherms were measured at 77 K, using Autosorb iQ2 adsorptometer, Quantachrome Instrument. Samples were degassed at 393 K for 12 h before measurements. The scanning electron microscope (SEM) images were acquired using the Hitachi SU-70. Transmission electron microscopic (TEM) images and elemental mapping were acquired by JEOL 2100PLUS instrument at an accelerating voltage of 200 kV. X-ray photoelectron spectroscopy (XPS) was performed on Thermo Scientific Escalab 250Xi with an Al-K α X-ray source. The binding energies of elements were calibrated using the C 1s photoelectron peak at 284.8 eV. The UV-vis absorption spectra were recorded from 200 – 1000 nm on a VARIAN UV-VIS-NIR spectrophotometer (Cary500). The UV-vis diffuse reflectance spectra were recorded using UV-Vis-NIR Spectrophotometer (Cary7000) with BaSO₄ used as a reference. The steady-state photoluminescence (PL) spectra were collected by a spectrometer (HR4000CG-UV-NIR, Ocean Optics). The electron spin resonance (ESR) was tested by a Bruker E-500 CW. 5,5-dimethyl-1-pyrroline N-oxide (DMPO) was used as spin-trapping reagents to detect O₂^{•-}. 2,2,6,6-Tetramethyl-4-piperidone hydrochloride (TEMP) was used as spin-trapping reagent to detect ¹O₂. The

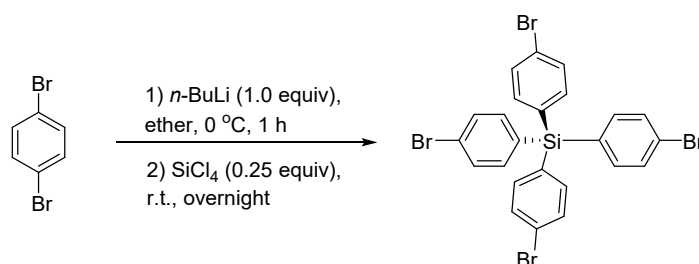
electrochemical impedance spectra (EIS), photocurrent response, of catalysts were measured on electrochemical workstation (CHI660E, CH Instruments, Shanghai, China).

1.3 Electrochemical measurements¹

All the photoelectrochemical measurements were obtained on an electrochemical workstation using a standard three-electrode cell at room temperature, the glass carbon electrode (GCE) was used as working electrode, a platinum wire electrode, and a saturated calomel electrode (SCE) as counter and reference electrode, respectively. A glassy carbon electrode was applied as the working electrode covered with a thin polymer film and 5 wt% Nafion for Mott-Schottky analysis, 0.1 M Na₂SO₄ aqueous solution was used as the electrolyte, and Mott-Schottky measurement was carried out at frequency of 1500 Hz, 2000 Hz and 2500 Hz with amplitude of 5 mV. The electrochemical impedance spectra (EIS) measurements were performed in 0.1 M KCl aqueous solution containing 5 mM [Fe (CN)₆]^{3-/4-} at room temperature, 7 μ L of slurry (5 mg powder, 225 μ L deionized water, 225 μ L EtOH and 50 μ L 1.5 wt% PVDF NMP solution) was covered to GCE as working electrode. The photocurrent measurements were performed with 7 μ L (5 mg powder was added into 1 mL EtOH and 10 μ L 5 wt% Nafion) of slurry covering the GCE as the working electrode. The visible light was generated by a 300 W Xe lamp. The electrolyte was 0.1 M Na₂SO₄ aqueous solution. The photocurrent measurements were recorded for 700 s under intermittent irradiation with a period of 50 s.

2. Synthesis of TEPS-4Br and TEPS-PAFs

2.1 Synthesis of tetrakis(4-bromophenyl) silane (TEPS-4Br)²



Scheme S1. Synthesis of TEPS-4Br.

Under a nitrogen atmosphere, *n*-butyllithium (1.6 M in hexane, 8.5 mL, 21.2 mmol) was added to a solution of 1,4-dibromobenzene (3.2 g, 13.6 mmol) in anhydrous ether (100.0 mL) at -78 °C, which was then stirred at 0 °C for 1 h. Then silicon tetrachloride (0.4 mL, 3.38 mmol) was added to the reaction mixture, which was subsequently warmed up at room temperature and stirred overnight.

The reaction mixture was quenched by adding deionized water (40.0 mL), which was then extracted with dichloromethane (3×20.0 mL). The organic layer was dried over MgSO_4 and evaporated to give an off-white powder, which was further purified by recrystallization in ethyl acetate (20.0 mL) to give TEPS-4Br product as a colorless solid (1.6 g, 2.46 mmol, 71%). ^1H NMR (500 MHz, CDCl_3 , 298 K) δ 7.54 (d, $J = 8.2$ Hz, 8H), 7.34 (d, $J = 8.2$ Hz, 8H) ppm.

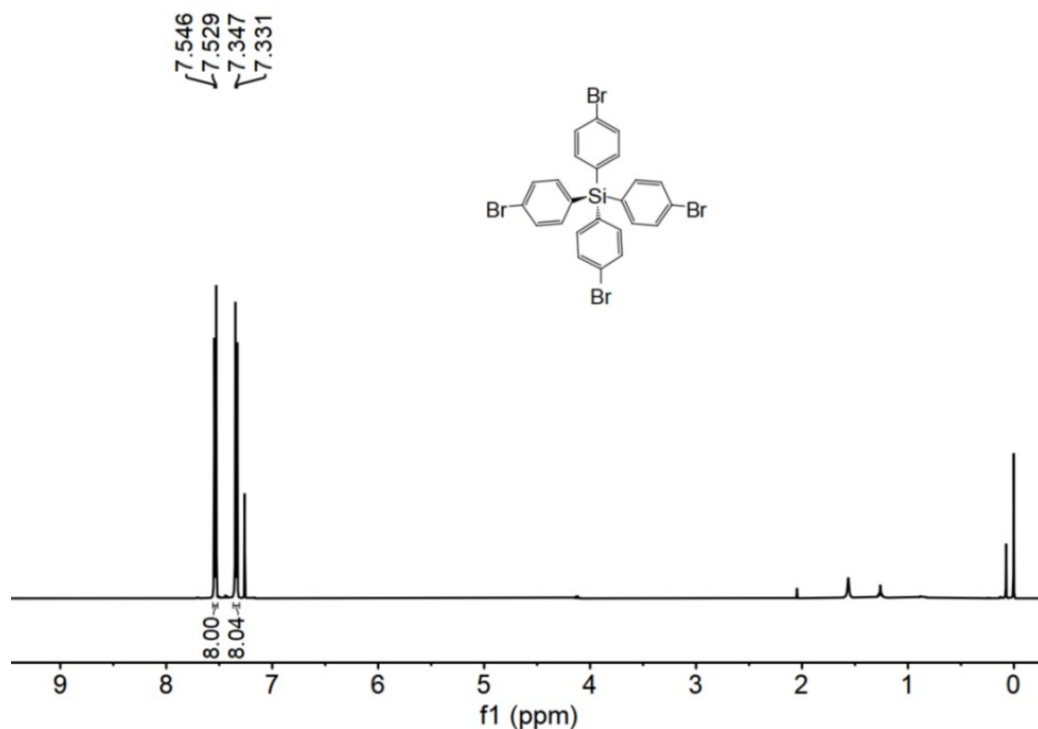
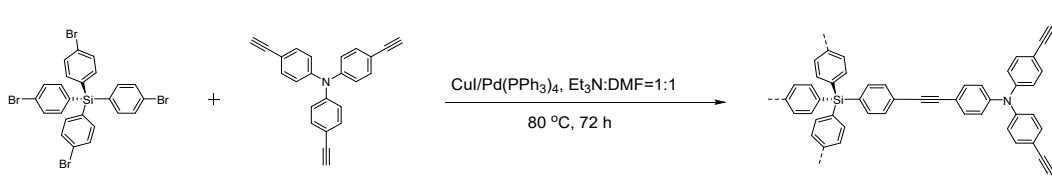


Fig. S1. ^1H NMR spectrum of TEPS-4Br.

2.2 Synthesis of PAF-403³

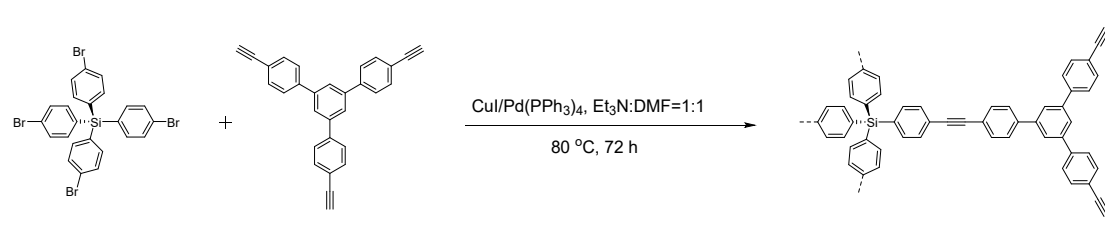


Scheme S2. Synthesis of PAF-403.

Under a nitrogen atmosphere, TEPS-4Br (202.2 mg, 0.31 mmol), tris(4-ethynylphenyl)amine (149.2 mg, 0.47 mmol), $\text{Pd}(\text{PPh}_3)_4$ (53.7 mg, 0.047 mmol), and CuI (17.7 mg, 0.093 mmol) were dissolved in anhydrous DMF (8.0 mL) and anhydrous Et_3N (8.0 mL) in a 100 mL Schlenk tube. The reaction mixture was stirred at 80 °C for 72 h. After cooling down to room temperature, the reaction mixture was filtered. The obtained solid was washed thoroughly with 2 M HCl , deionized water,

EtOH, CH₂Cl₂, THF and followed by Soxhlet extraction for 24 h with THF and CH₂Cl₂ solution respectively. The resulting solid was collected and then dried in vacuum oven at 100 °C to give a dark brown solid powder (261.2 mg, 76%).

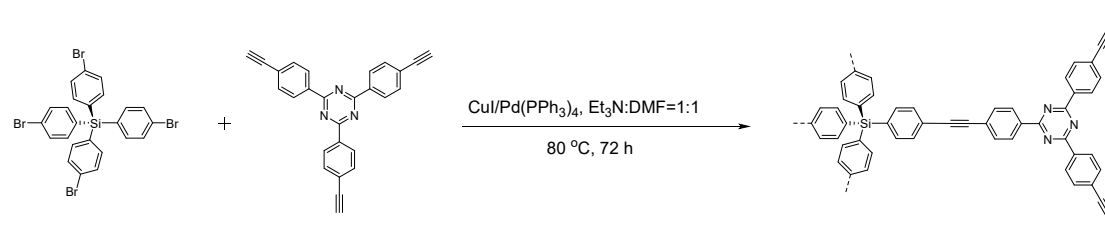
2.3 Synthesis of PAF-404³



Scheme S3. Synthesis of **PAF-404**.

Under a nitrogen atmosphere, TEPS-4Br (202.2 mg, 0.31 mmol), 1,3,5-tris(4-ethynylphenyl)benzene (177.9 mg, 0.47 mmol), Pd(PPh₃)₄ (53.7 mg, 0.047 mmol), and CuI (17.7 mg, 0.093 mmol) were dissolved in anhydrous DMF (8.00 mL) and anhydrous Et₃N (8.0 mL) in a 100 mL Schlenk tube. The reaction mixture was stirred at 80 °C for 72 h. After cooling down to room temperature, the reaction mixture was filtered. The obtained solid was washed thoroughly with 2 M HCl, deionized water, EtOH, CH₂Cl₂, THF and followed by Soxhlet extraction for 24 h with THF and CH₂Cl₂ solution respectively. The resulting solid was collected and then dried in vacuum oven at 100 °C to give a yellow solid powder (268.1 mg, 72%).

2.4 Synthesis of PAF-405³



Scheme S4. Synthesis of **PAF-405**.

Under a nitrogen atmosphere, TEPS-4Br (202.2 mg, 0.31 mmol), 2,4,6-tris(4-ethynylphenyl)-1,3,5-triazine (179.3 mg, 0.47 mmol), Pd(PPh₃)₄ (53.7 mg, 0.047 mmol), and CuI (17.7 mg, 0.093 mmol) were dissolved in anhydrous DMF (8.0 mL) and anhydrous Et₃N (8.0 mL) in a 100 mL Schlenk tube. The reaction mixture was stirred at 80 °C for 72 h. After cooling down to room temperature, the reaction mixture was filtered. The obtained solid was washed thoroughly with 2 M HCl, deionized water, EtOH, CH₂Cl₂, THF and followed by Soxhlet extraction for 24 h with THF

and CH₂Cl₂ solution respectively. The resulting solid was collected and then dried in vacuum oven at 100 °C to give a yellow solid powder (261.8 mg, 70%).

3. Typical procedure for photocatalytic C-3 thialocyanation of indoles

Photocatalyst (1.0-5.0 mg), indole or its derivatives (0.5 mmol), NH₄SCN (1.0 mmol) and solvent (5.0 mL) were added into a glass vial. The reaction mixture was stirred in the open air at room temperature under the irradiation of 25 W blue LEDs (420 nm). After the reaction was completed, the catalyst was removed from reaction mixture by filtration and thoroughly washed with THF. After all the volatiles in the combined filtrates were removed under reduced pressure, the obtained crude product was further purified by flash column chromatography (petroleum/ethyl acetate = 5/1~2/1 as eluent) to give 3-thiocyanated indoles and their derivatives.

4. Recycling experiment

After the first run of catalytic reaction was finished, PAF-405 catalyst was removed from reaction mixture by filtration, and thoroughly washed with CH₂Cl₂ and THF, and dried in vacuo at 100 °C overnight. The recycled PAF-405 photocatalyst was reused for the next cycle under identical conditions.

5. Computational details

DFT calculations were carried out by **Gaussian 16 software package**.⁴ All fragments of PAF-403, PAF-404 and PAF-405 were optimized at the B3LYP/6-31G(d) level.^{5,6} Vibrational frequency calculations were performed to confirm their stability. The distribution of HOMO-LUMO orbitals was calculated using the Multiwfn 3.8 software and visualized by Visual Molecular Dynamics (VMD) software.

6. PXRD patterns

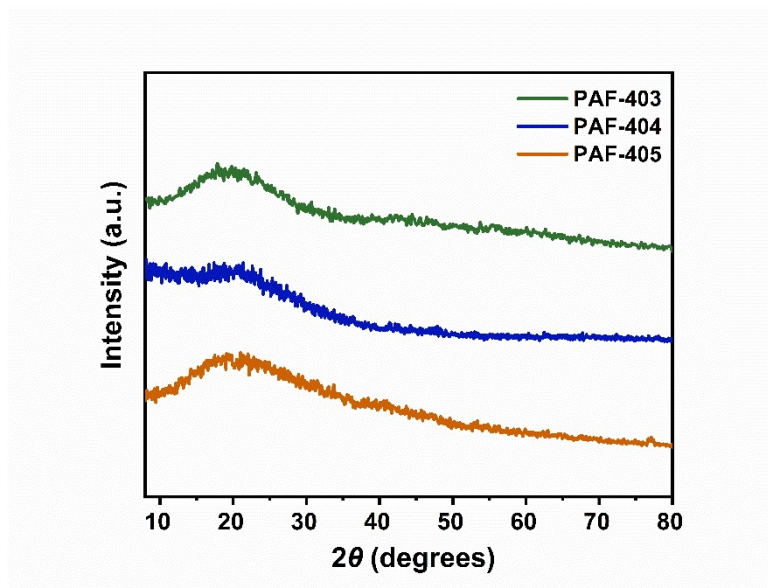


Fig. S2. PXRD patterns of PAF-403, PAF-404, and PAF-405.

7. N₂ adsorption/desorption isotherms

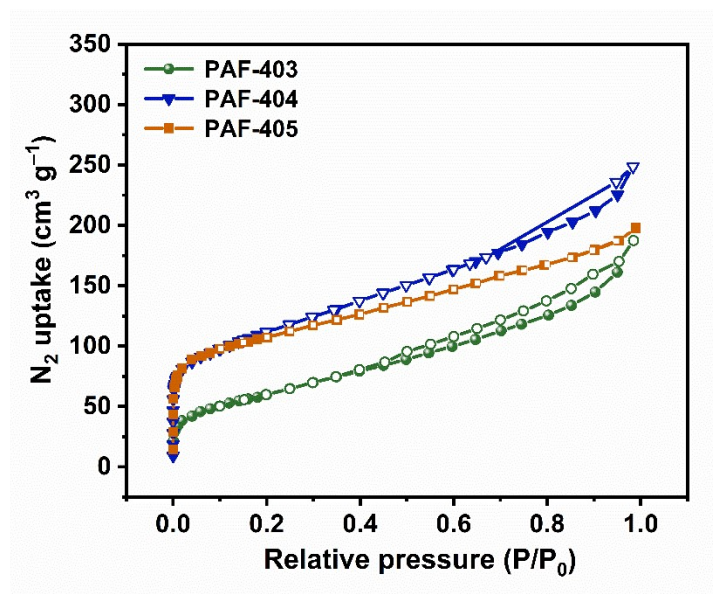


Fig. S3. N₂ adsorption/desorption isotherms at 77 K of TEPS-PAFs.

Comment: The relatively lower surface area of PAF-405 may be attributed to the intermolecular hydrogen bonding interactions and π - π stacking effects between triazine units in the framework, which partially block the pores and consequently reduce the specific surface area.

8. Pore size distribution

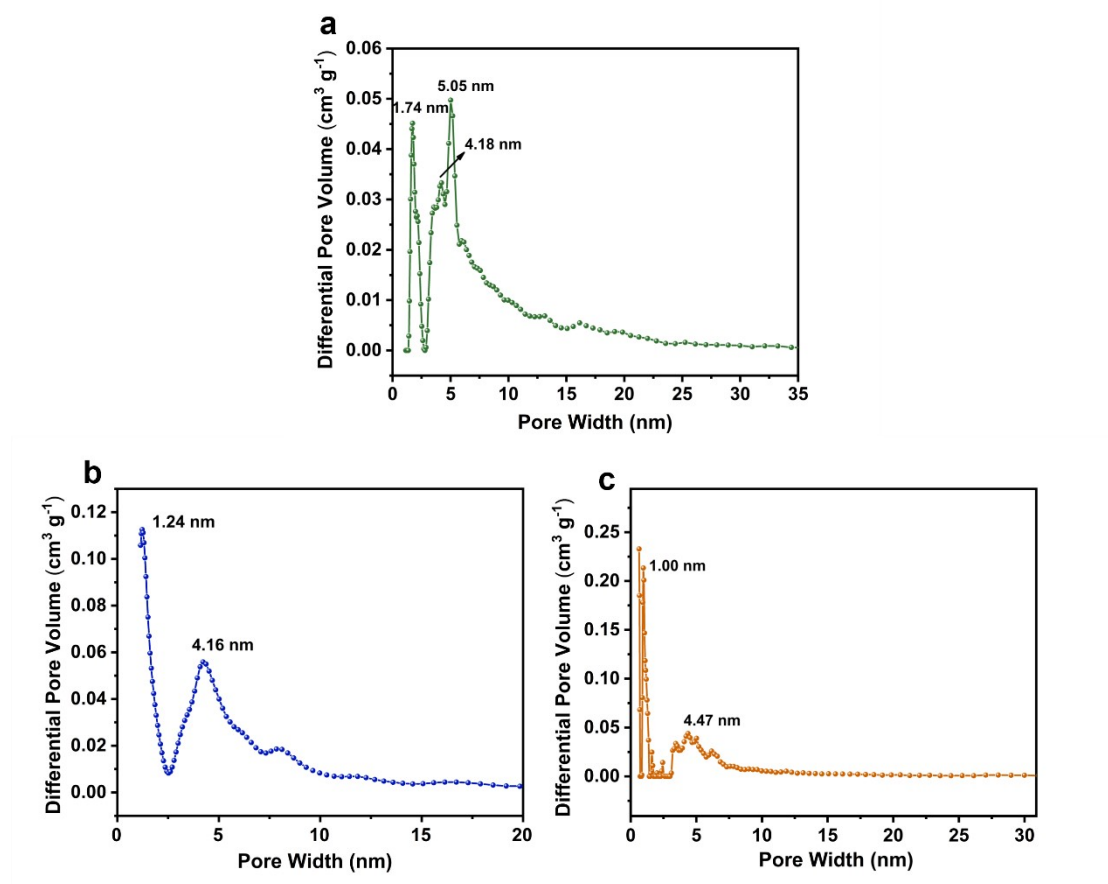


Fig. S4. The pore size distribution of PAF-403 (a) PAF-404 (b), and PAF-405 (c). (The pore size distributions were evaluated by using NLDFT method.)

9. TGA curves

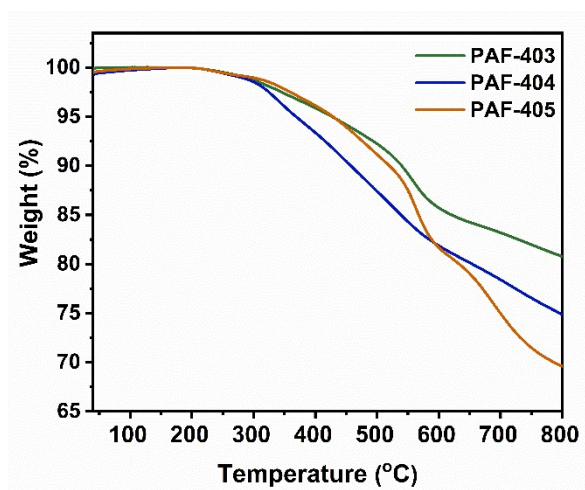


Fig. S5. TGA curves of TEPS-PAFs.

10. SEM images

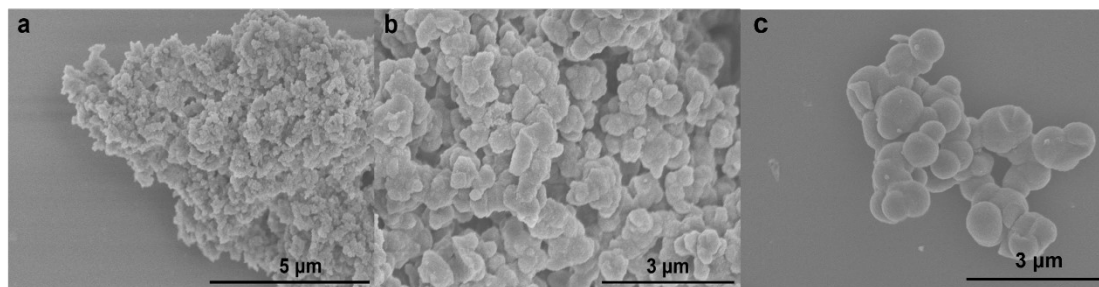


Fig. S6. SEM images of PAF-403 (a), PAF-404 (b) and PAF-405 (c).

11. TEM image

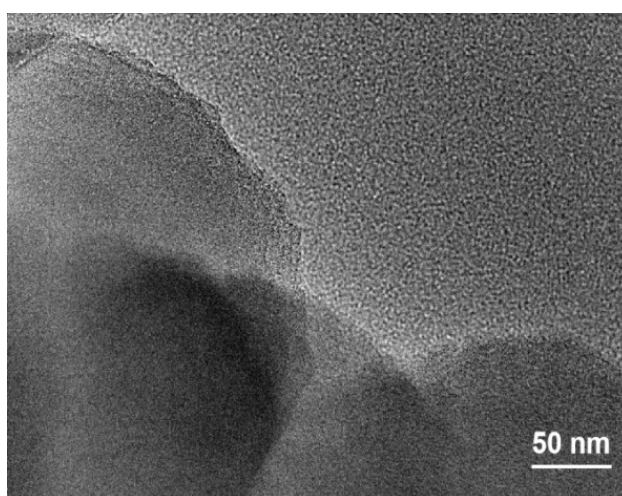


Fig. S7. TEM image of PAF-405.

12. TEM elemental mapping

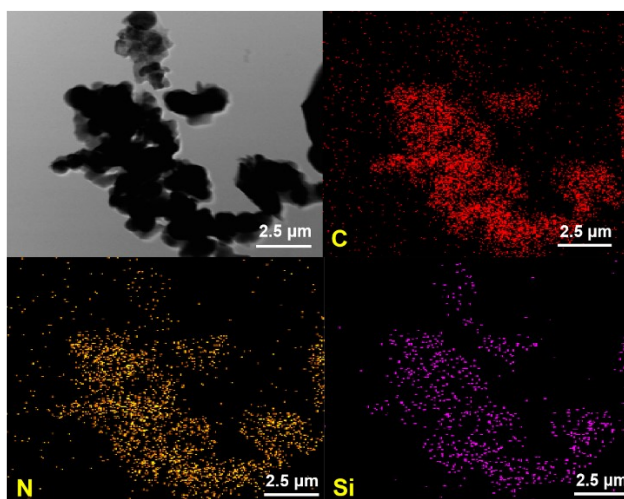


Fig. S8. TEM elemental mapping of PAF-405 for carbon (red), nitrogen (yellow) and silicon (purple).

13. XPS spectra

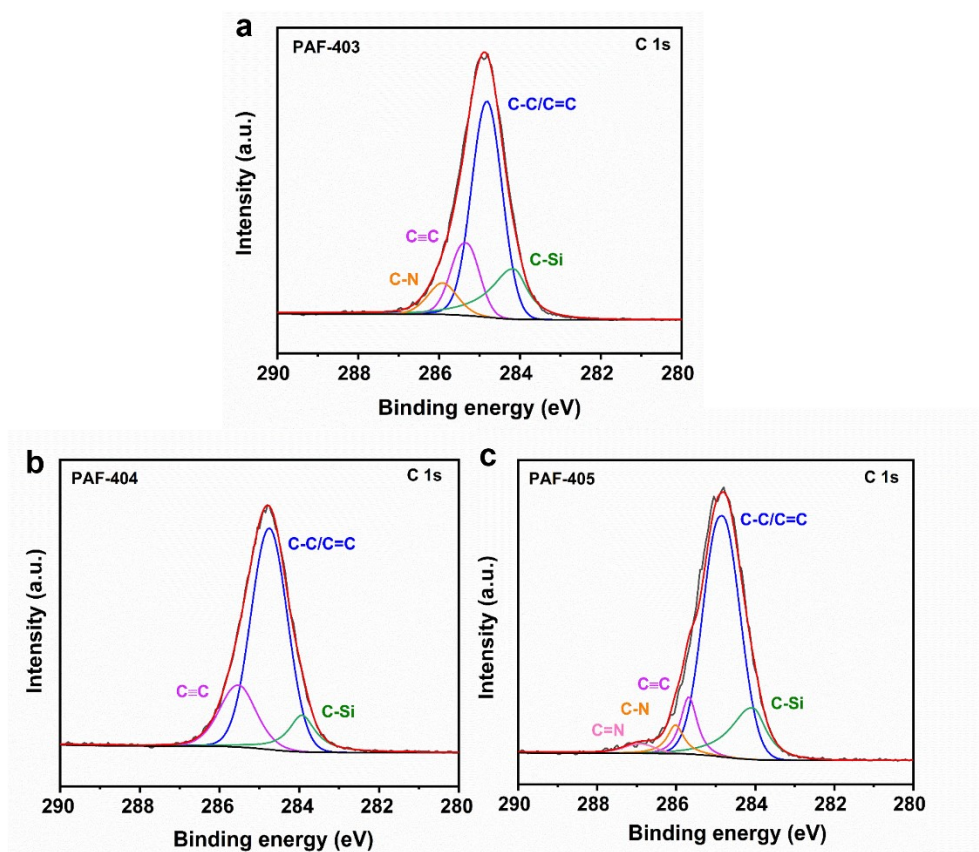


Fig. S9. High-resolution C 1s XPS spectra of PAF-403 (a) PAF-404 (b), and PAF-405 (c).

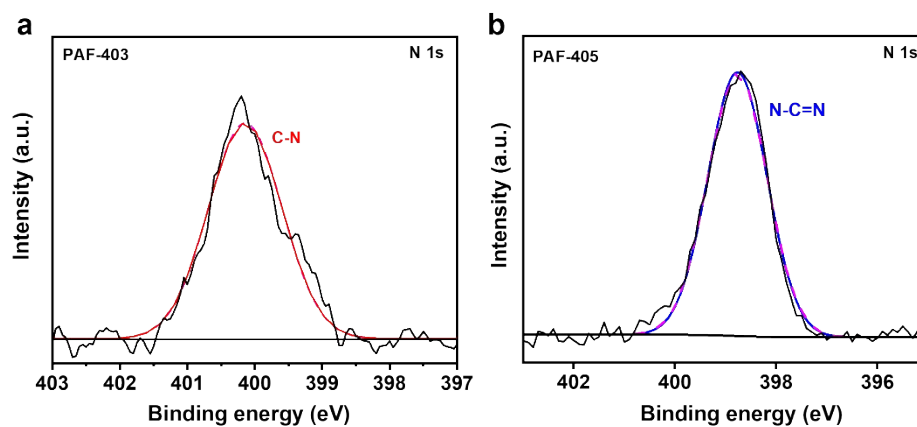


Fig. S10. High-resolution N 1s XPS spectra of (a) PAF-403 and (b) PAF-405.

14. Tauc plots

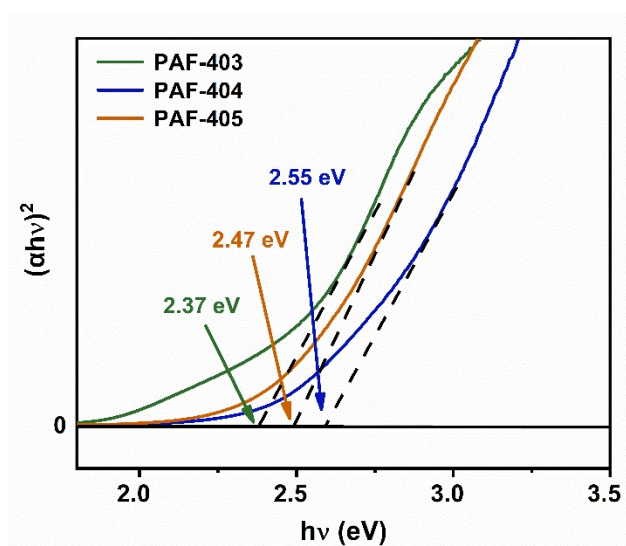


Fig. S11. Tauc plots of TEPS-PAFs.

15. VB-XPS spectra

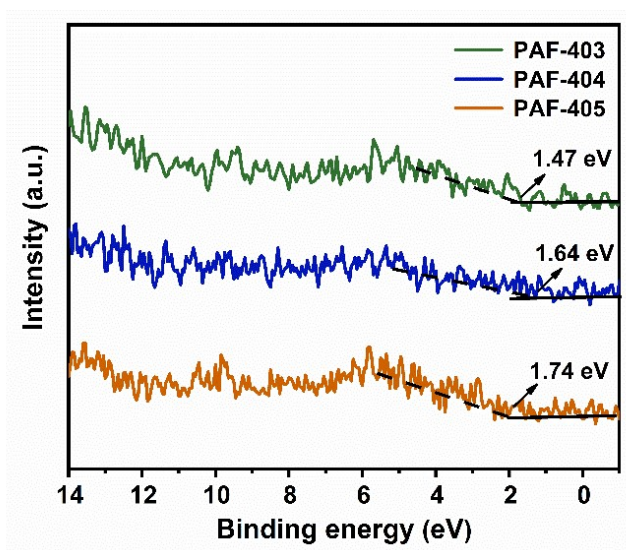


Fig. S12. VB-XPS spectra of TEPS-PAFs.

16. PL spectra

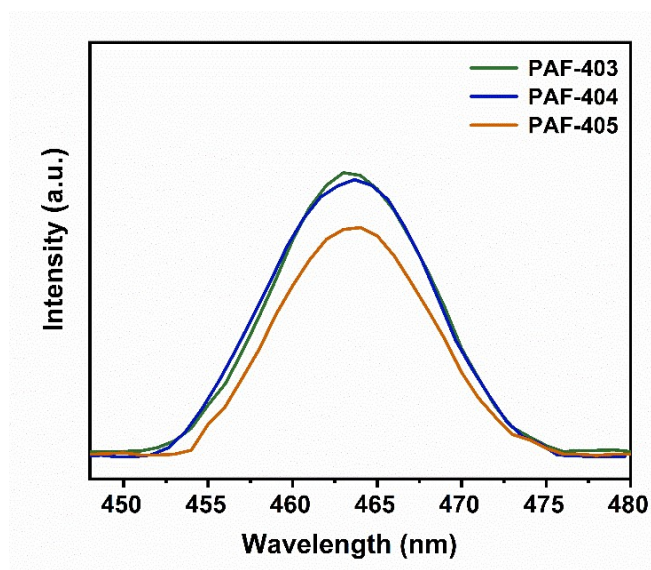


Fig. S13. PL spectra of PAF-403, PAF-404, and PAF-405.

17. Time-resolved fluorescence spectra

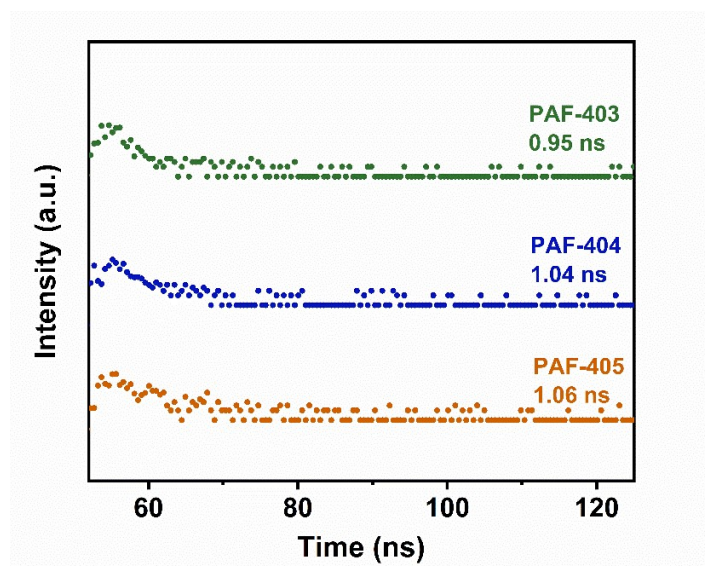
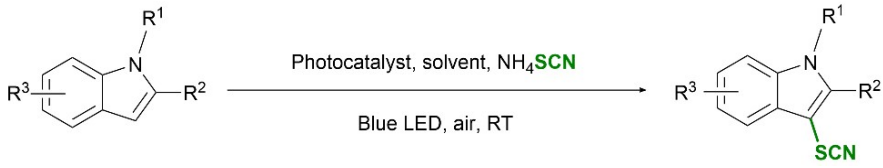


Fig. S14. Time-resolved fluorescence spectra of TEPS-PAFs.

18. Supplementary tables

Table S1. Photocatalytic C-3 thiocyanation of indoles by TEPS-PAFs ^a

				
entry	catalyst	hν	solvent	Yield ^b
1	PAF-403 (5.0 mg)	Blue LED (420 nm)	THF	74%
2	PAF-404 (5.0 mg)	Blue LED (420 nm)	THF	68%
3	PAF-405 (5.0 mg)	Blue LED (420 nm)	THF	99%
4	PAF-405 (1.0 mg)	Blue LED (420 nm)	THF	62%
5	PAF-405 (2.0 mg)	Blue LED (420 nm)	THF	70%
6	PAF-405 (3.0 mg)	Blue LED (420 nm)	THF	83%
7	PAF-405 (5.0 mg)	Blue LED (420 nm)	Acetone	21%
8	PAF-405 (5.0 mg)	Blue LED (420 nm)	CH ₂ Cl ₂	17%
9	PAF-405 (5.0 mg)	Blue LED (420 nm)	DMF	12%
10	PAF-405 (5.0 mg)	Blue LED (420 nm)	CH ₃ CN	56%
11	PAF-405 (5.0 mg)	Blue LED (420 nm)	CH ₃ OH	31%
12	PAF-405 (5.0 mg)	Blue LED (460 nm)	THF	88%
13	PAF-405 (5.0 mg)	Green LED (500 nm)	THF	75%
14	PAF-405 (5.0 mg)	Red LED (620 nm)	THF	52%

^a Reaction conditions: TEPS-PAFs (5.0 mg), substrate (0.5 mmol), NH₄SCN (1.0 mmol), solvent (5.0 mL), air, 25 °C. ^b Isolated yield.

Comment: The evaluation of photocatalytic activity should consider a comprehensive analysis of optical and electronic characterizations such as UV-visible diffuse reflectance spectroscopy,

transient photocurrent response, and electrochemical impedance spectroscopy. Compared with PAF-403, PAF-404 exhibits a narrow range of light absorption, lower transient photocurrent response, and higher electrochemical impedance. Additionally, theoretical calculations reveal that the HOMO and LUMO orbital distributions and electrostatic potential analysis of PAF-403 demonstrate a stronger D- π -A effect compared to PAF-404, indicating superior charge separation efficiency in PAF-403. This comprehensive evaluation may account for superior catalytic activity of PAF-403 compared to PAF-404.

Table S2. A comparison of photocatalytic performance of TEPS-PAFs with reported photocatalysts.

Entry	Material	h ν	Substrate	Atmosphere	Time (h)	Yield (%)	Reference
1	MeO-TBT-COF	Blue LED	0.24 mmol	O ₂	8 h	95%	7
2	0.45%N-ZnO	Blue LED	0.5 mmol	Air	16 h	94%	8
3	TP-PB COF	Blue LED	0.24 mmol	Air	8 h	97%	9
4	ARS-TiO ₂	Blue LED	1 mmol	O ₂	20 h	93%	10
5	COF-JLU24	Blue LED	0.3 mmol	O ₂	7 h	95%	11
6	Rose Bengal	14 W CFL	0.5 mmol	Air	18 h	100%	12
7	PM-PM-COF	Blue LED	0.24 mmol	Air	8 h	96%	13
8	Cbz-CMP-9	Blue LED	0.25 mmol	O ₂	4 h	98%	14
9	CMP-CSU6	14 W LED	0.5 mmol	O ₂	10 h	95%	15
10	Cs ₂ AgBiBr ₆	Blue LED	0.2 mmol	Air	20 h	97%	16
11	EDOT-COP	Blue LED	0.5 mmol	Air	3-10 h	99%	17
12	PDI-COF	White LED	0.4 mmol	Air	48 h	97%	18
13	SiMo-NDI	White LED	0.5 mmol	Air	24 h	94%	19
14	PAF-403	Blue LED	0.5 mmol	Air	10 h	72%	This work
15	PAF-404	Blue LED	0.5 mmol	Air	10 h	65%	
16	PAF-405	Blue LED	0.5 mmol	Air	10 h	99%	

19. Scavenger experiments

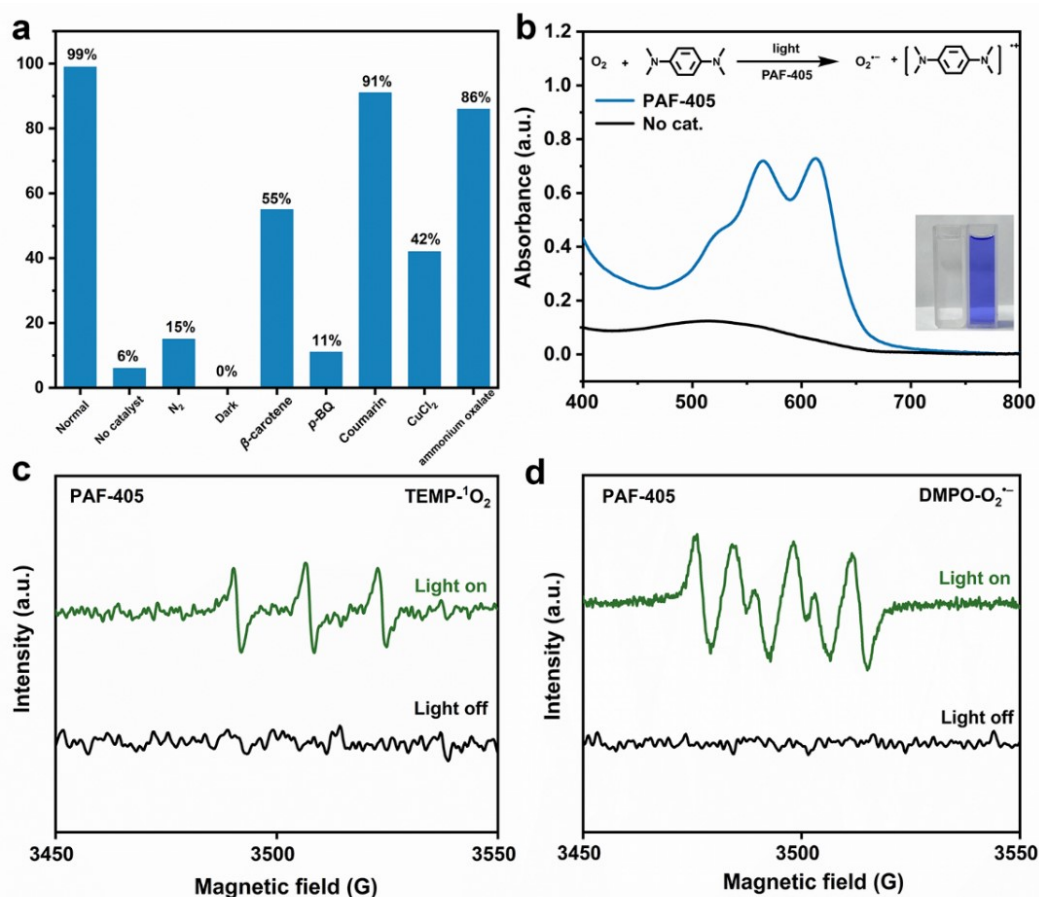


Fig. S15. (a) Control experiments using PAF-405 catalyst under various conditions (β -carotene as the singlet oxygen scavenger, *p*-BQ as the superoxide scavenger, coumarin as the hydroxyl radical scavenger, CuCl₂ as the electron scavenger and ammonium oxalate as the hole scavenger); (b) UV-Vis absorption spectra of TMPD in THF in the absence (black curve) or presence (blue curve) of PAF-405 under light irradiation in the open air; ESR spectra of TEMP-¹O₂ (c) and DMPO-O₂^{•-} (d) trapping experiments in the presence of PAF-405 under light irradiation.

20. Recyclability of PAF-405

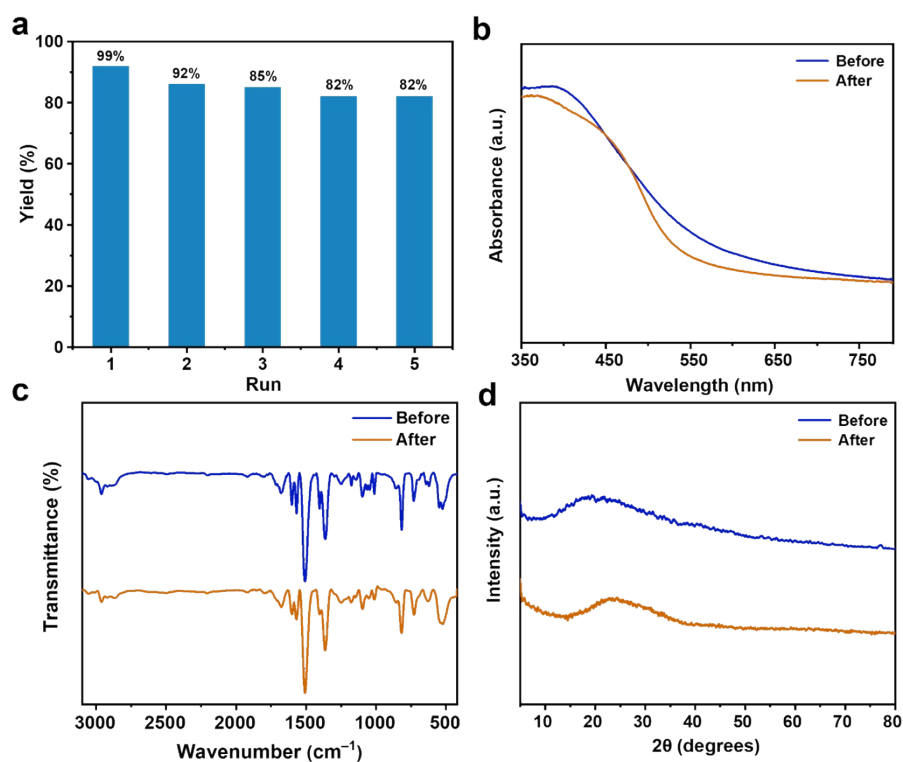
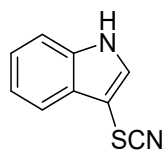
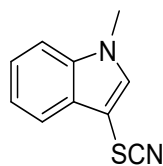


Fig. S16. (a) Reusability of PAF-405 in the photocatalytic C-3 thiocyanation of indoles; UV/Vis reflectance spectra (b), FT-IR spectra (c), and PXRD spectra (d) of photocatalyst PAF-405 before and after five cycles.

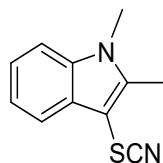
NMR data



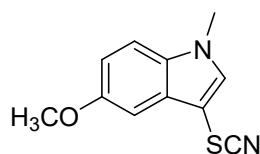
3-thiocyanato-1H-indole (2a): ^1H NMR (500 MHz, Chloroform-*d*, 298 K) δ 8.69 (s, 1H), 7.73 – 7.66 (m, 1H), 7.34 – 7.26 (m, 2H), 7.24 – 7.18 (m, 2H) ppm. ^{13}C NMR (126 MHz, Chloroform-*d*, 298 K) δ 136.04, 131.17, 127.62, 123.80, 121.84, 118.59, 112.31, 112.22, 91.67 ppm.



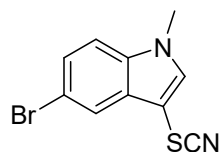
1-Methyl-3-thiocyanato-1H-indole (2b): ^1H NMR (500 MHz, Chloroform-*d*, 298 K) δ 7.82 (d, J = 7.9 Hz, 1H), 7.44 – 7.32 (m, 4H), 3.84 (s, 3H) ppm. ^{13}C NMR (126 MHz, Chloroform-*d*, 298 K) δ 136.16, 134.04, 127.48, 122.43, 120.60, 117.95, 110.84, 109.18, 88.92, 32.41 ppm.



1,2-Dimethyl-3-thiocyanato-1H-indole (2c): ^1H NMR (500 MHz, Chloroform-*d*, 298 K) δ 7.82 – 7.76 (m, 1H), 7.35 (d, J = 2.8 Hz, 3H), 3.66 (s, 3H), 2.60 (s, 3H) ppm. ^{13}C NMR (126 MHz, Chloroform-*d*, 298 K) δ 143.38, 136.72, 128.13, 122.49, 121.30, 117.99, 111.86, 109.52, 87.55, 30.28, 10.85 ppm.



5-Methoxy-1-Methyl-3-thiocyanato-1H-indole (2d): ^1H NMR (500 MHz, Chloroform-*d*, 298 K) δ 7.34 (s, 1H), 7.27 (d, J = 8.9 Hz, 1H), 7.23 (d, J = 2.4 Hz, 1H), 7.02 (dd, J = 8.9, 2.5 Hz, 1H), 3.96 (s, 3H), 3.74 (s, 3H) ppm. ^{13}C NMR (126 MHz, Chloroform-*d*, 298 K) δ 154.73, 134.24, 131.17, 128.28, 113.13, 110.92, 110.18, 98.96, 87.97, 54.83, 32.58 ppm.

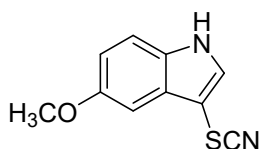


5-Bromo-1-Methyl-3-thiocyanato-1H-indole (2e): ^1H NMR (500 MHz, Chloroform-*d*, 298 K) δ

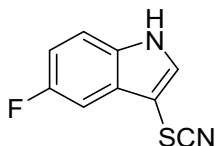
7.89 (d, $J = 1.9$ Hz, 1H), 7.44 – 7.37 (m, 2H), 7.22 (d, $J = 5.4$ Hz, 1H), 3.80 (s, 3H) ppm. ^{13}C NMR (126 MHz, Chloroform- d , 298 K) δ 136.44, 136.24, 130.49, 126.94, 122.01, 115.69, 112.08, 34.00 ppm.



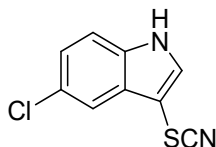
5-Methyl-3-thiocyanato-1H-indole (2f): ^1H NMR (500 MHz, Chloroform- d , 298 K) δ 8.46 (s, 1H), 7.51 (s, 1H), 7.39 (d, $J = 1.7$ Hz, 1H), 7.24 (d, $J = 8.4$ Hz, 1H), 7.07 (d, $J = 8.3$ Hz, 1H), 2.44 (s, 3H) ppm. ^{13}C NMR (126 MHz, Chloroform- d , 298 K) δ 133.28, 130.59, 129.85, 126.93, 124.59, 117.36, 110.89, 110.67, 90.75, 20.49 ppm.



5-Methoxy-3-thiocyanato-1H-indole (2g): ^1H NMR (500 MHz, Chloroform- d , 298 K) δ 8.78 (s, 1H), 7.42 (d, $J = 2.8$ Hz, 1H), 7.28 (d, $J = 8.9$ Hz, 1H), 7.18 (d, $J = 2.5$ Hz, 1H), 6.94 (dd, $J = 8.8$, 2.4 Hz, 1H), 3.91 (s, 3H) ppm. ^{13}C NMR (126 MHz, Chloroform- d , 298 K) δ 154.73, 130.41, 129.81, 127.49, 113.50, 112.03, 111.05, 98.77, 90.41, 54.82 ppm.

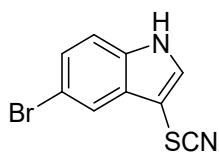


5-Fluoro-3-thiocyanato-1H-indole (2h): ^1H NMR (500 MHz, Chloroform- d , 298 K) δ 8.73 (s, 1H), 7.55 (d, $J = 2.9$ Hz, 1H), 7.44 (dd, $J = 8.8$, 2.5 Hz, 1H), 7.36 (dd, $J = 8.9$, 4.2 Hz, 1H), 7.05 (td, $J = 9.0$, 2.5 Hz, 1H) ppm. ^{13}C NMR (126 MHz, Chloroform- d , 298 K) δ 160.03, 158.14, 132.60, 132.44, 128.54 (d, $J = 10.1$ Hz), 113.19, 113.12, 112.81, 112.60, 111.66, 104.18, 103.98, 92.50 (d, $J = 4.9$ Hz) ppm.

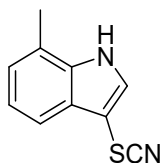


5-Chloro-3-thiocyanato-1H-indole (2i): ^1H NMR (500 MHz, Chloroform- d , 298 K) δ 8.77 (s, 1H), 7.84 (d, $J = 2.0$ Hz, 1H), 7.62 (d, $J = 2.8$ Hz, 1H), 7.41 (s, 1H), 7.37 – 7.31 (m, 1H) ppm. ^{13}C NMR (126 MHz, Chloroform- d , 298 K) δ 134.19, 132.03, 128.70, 127.90, 124.39, 118.27, 113.03, 111.28,

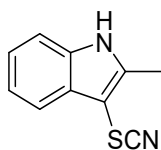
92.26 ppm.



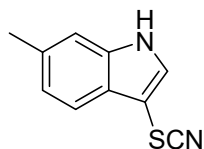
5-Bromo-3-thiocyanato-1H-indole (2j): ^1H NMR (500 MHz, Chloroform-*d*, 298 K) δ 8.71 (s, 1H), 7.94 (s, 1H), 7.54 (d, J = 2.9 Hz, 1H), 7.41 (dd, J = 8.6, 1.8 Hz, 1H), 7.31 (d, J = 8.7 Hz, 1H) ppm. ^{13}C NMR (126 MHz, Chloroform-*d*, 298 K) δ 134.36, 131.72, 129.12, 126.82, 121.25, 115.21, 113.24, 111.06, 92.09 ppm.



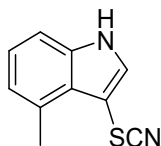
7-Methyl-3-thiocyanato-1H-indole (2k): ^1H NMR (500 MHz, Chloroform-*d*, 298 K) δ 8.66 (s, 1H), 7.64 (d, J = 8.0 Hz, 1H), 7.48 (d, J = 2.9 Hz, 1H), 7.23 (dd, J = 14.8, 7.3 Hz, 1H), 7.11 (d, J = 7.1 Hz, 1H), 2.47 (s, 3H) ppm. ^{13}C NMR (126 MHz, Chloroform-*d*, 298 K) δ 134.59, 129.64, 126.29, 123.36, 121.05, 120.39, 115.35, 111.02, 91.52, 15.31 ppm.



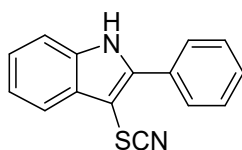
2-Methyl-3-thiocyanato-1H-indole (2l): ^1H NMR (500 MHz, Chloroform-*d*, 298 K) δ 8.43 (s, 1H), 7.71 – 7.65 (m, 1H), 7.32 (dd, J = 6.9, 2.4 Hz, 1H), 7.29 – 7.20 (m, 2H), 2.56 (d, J = 2.1 Hz, 3H) ppm. ^{13}C NMR (126 MHz, Chloroform-*d*, 298 K) δ 140.83, 134.05, 127.74, 122.05, 120.63, 117.20, 110.75, 110.10, 88.37, 11.14 ppm.



5-Methyl-3-thiocyanato-1H-indole (2m): ^1H NMR (500 MHz, Chloroform-*d*, 298 K) δ 8.49 (s, 1H), 7.67 (d, J = 8.1 Hz, 1H), 7.42 (d, J = 2.6 Hz, 1H), 7.23 (d, J = 19.7 Hz, 1H), 7.14 (d, J = 8.2 Hz, 1H), 2.48 (s, 3H) ppm. ^{13}C NMR (126 MHz, Chloroform-*d*, 298 K) δ 136.50, 134.06, 130.29, 125.56, 123.77, 118.43, 111.93, 111.91, 92.22, 21.70 ppm.



4-Methyl-3-thiocyanato-1H-indole (2n): ^1H NMR (500 MHz, Chloroform-*d*, 298 K) δ 8.52 (s, 1H), 7.44 (d, $J = 2.9$ Hz, 1H), 7.21 – 7.16 (m, 1H), 7.14–7.07 (m, 1H), 6.96 – 6.91 (m, 1H), 2.86 (s, 3H) ppm. ^{13}C NMR (126 MHz, Chloroform-*d*, 298 K) δ 135.42, 130.99, 130.12, 124.58, 123.01, 122.54, 112.16, 108.96, 91.43, 18.17 ppm.



2-Phenyl-3-thiocyanato-1H-indole (2o): ^1H NMR (500 MHz, Chloroform-*d*, 298 K) δ 8.60 (s, 1H), 7.81 – 7.74 (m, 1H), 7.67 (dd, $J = 6.9, 1.6$ Hz, 2H), 7.48 (d, $J = 7.7$ Hz, 4H), 7.30 – 7.23 (m, 2H) ppm. ^{13}C NMR (126 MHz, Chloroform-*d*, 298 K) δ 143.15, 135.44, 130.08, 129.77, 129.68, 129.20, 128.68, 124.18, 122.21, 119.18, 111.84, 111.64, 89.40 ppm.

NMR spectra

^1H and ^{13}C Spectra of compound 2a (CDCl₃)

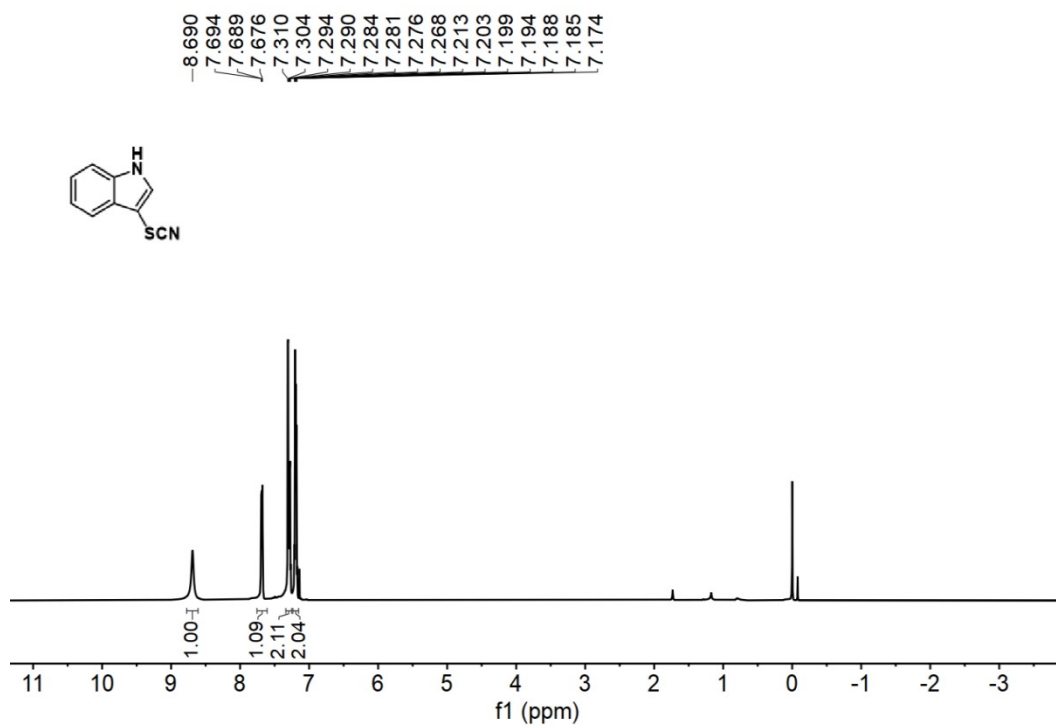


Fig. S17. ^1H NMR (500 MHz, Chloroform-*d*, 298 K) spectrum of **2a** in CDCl₃.

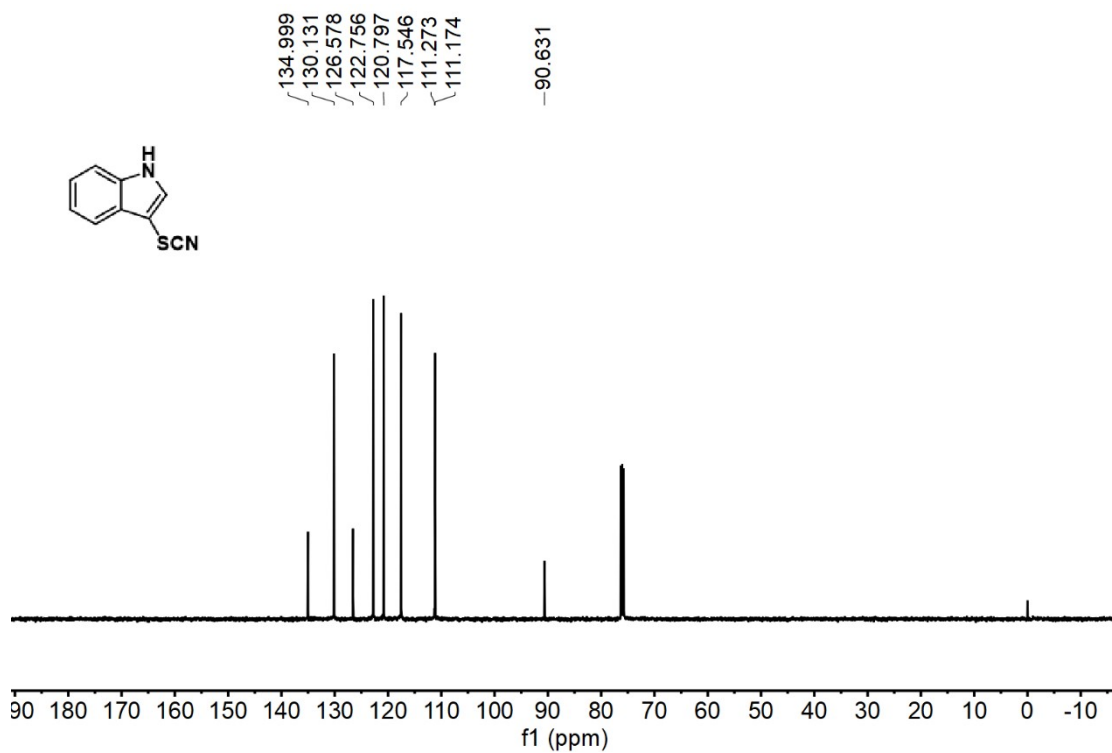


Fig. S18. ¹³C NMR (126 MHz, Chloroform-*d*, 298 K) spectrum of **2a** in CDCl₃.

¹H and ¹³C Spectra of compound 2b (CDCl₃)

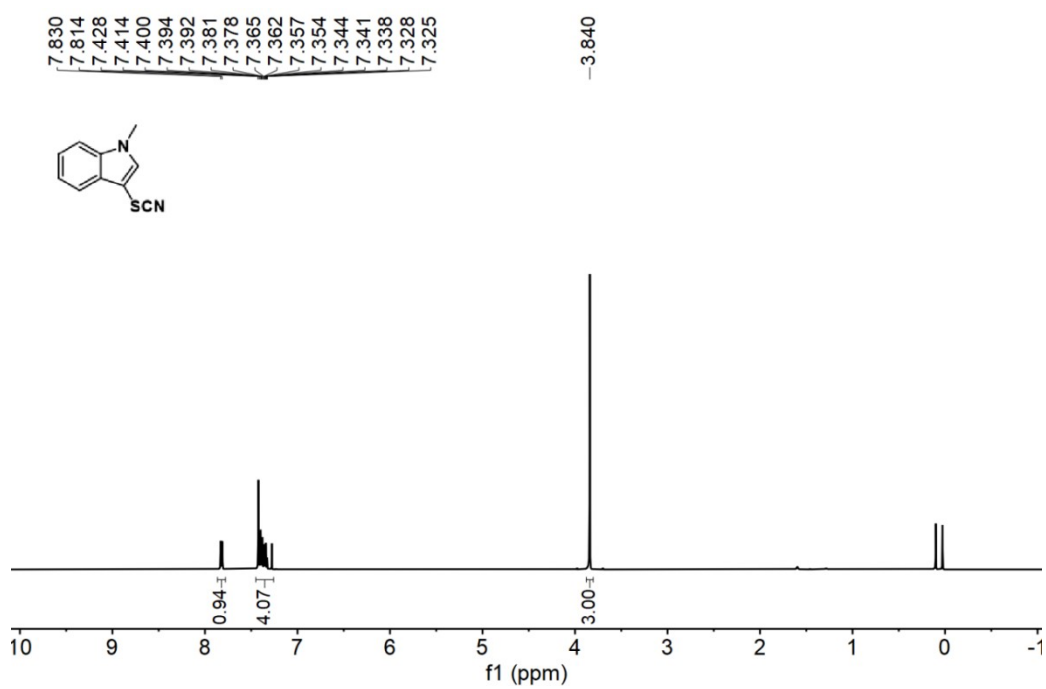


Fig. S19. ¹H NMR (500 MHz, Chloroform-*d*, 298 K) spectrum of **2b** in CDCl₃.

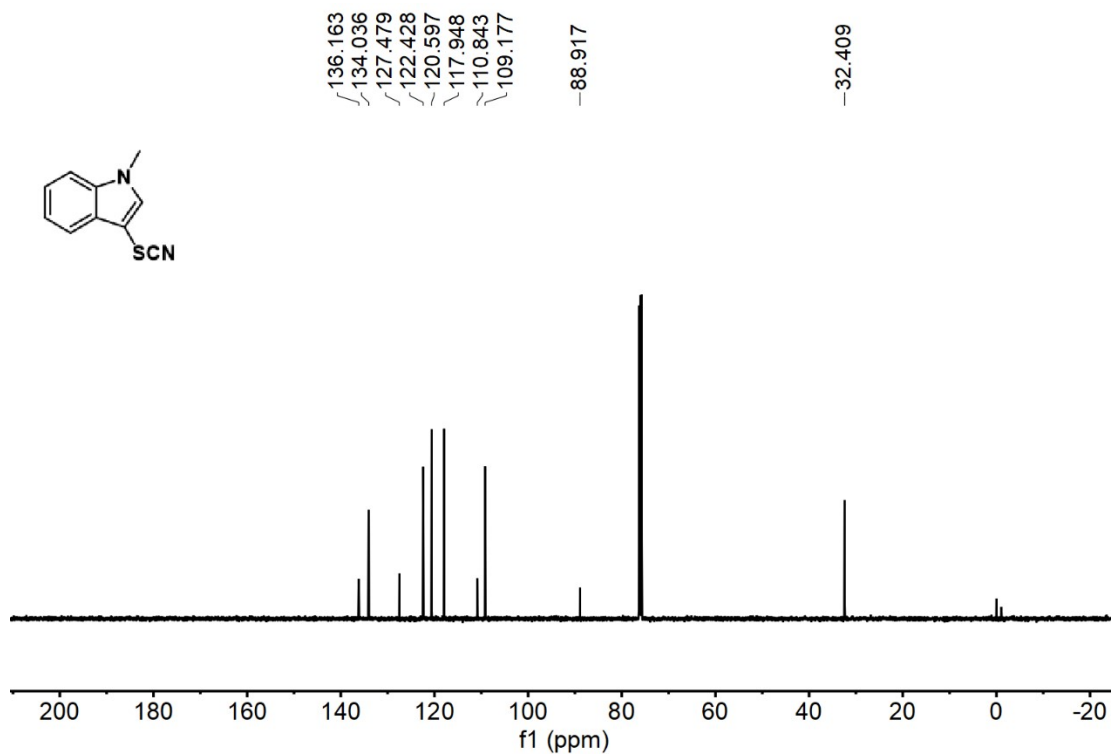


Fig. S20. ¹³C NMR (126 MHz, Chloroform-*d*, 298 K) spectrum of **2b** in CDCl₃.

¹H and ¹³C Spectra of compound 2c (CDCl₃)

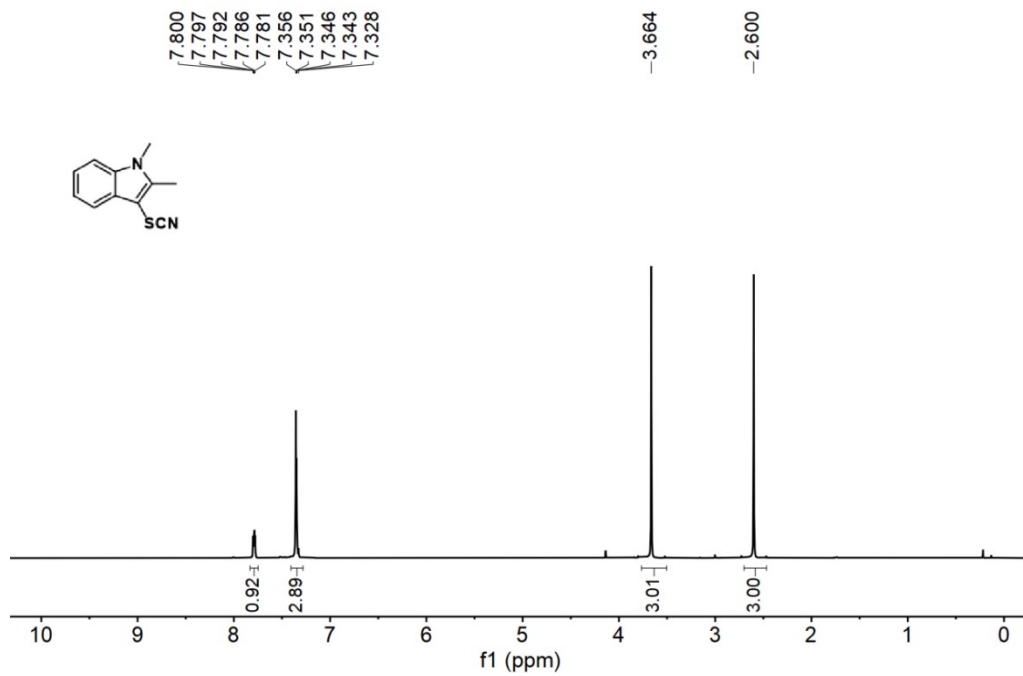


Fig. S21. ¹H NMR (500 MHz, Chloroform-*d*, 298 K) spectrum of **2c** in CDCl₃.

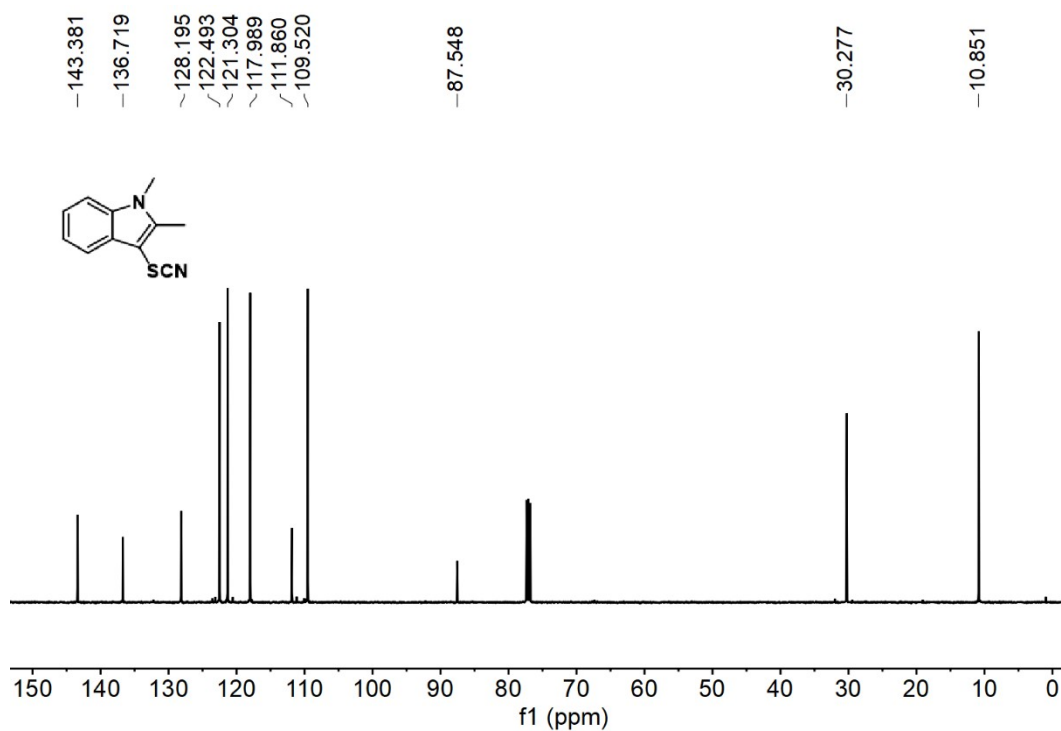


Fig. S22. ¹³C NMR (126 MHz, Chloroform-*d*, 298 K) spectrum of **2c** in CDCl₃.

¹H and ¹³C Spectra of compound 2d (CDCl₃)

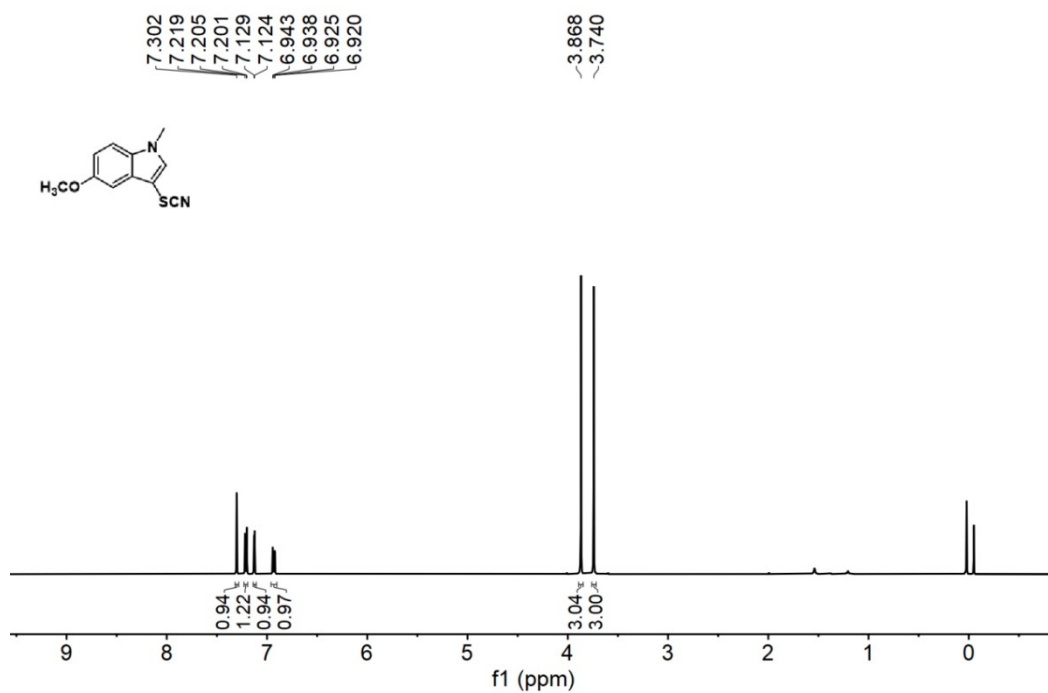


Fig. S23. ¹H NMR (500 MHz, Chloroform-*d*, 298 K) spectrum of **2d** in CDCl₃.

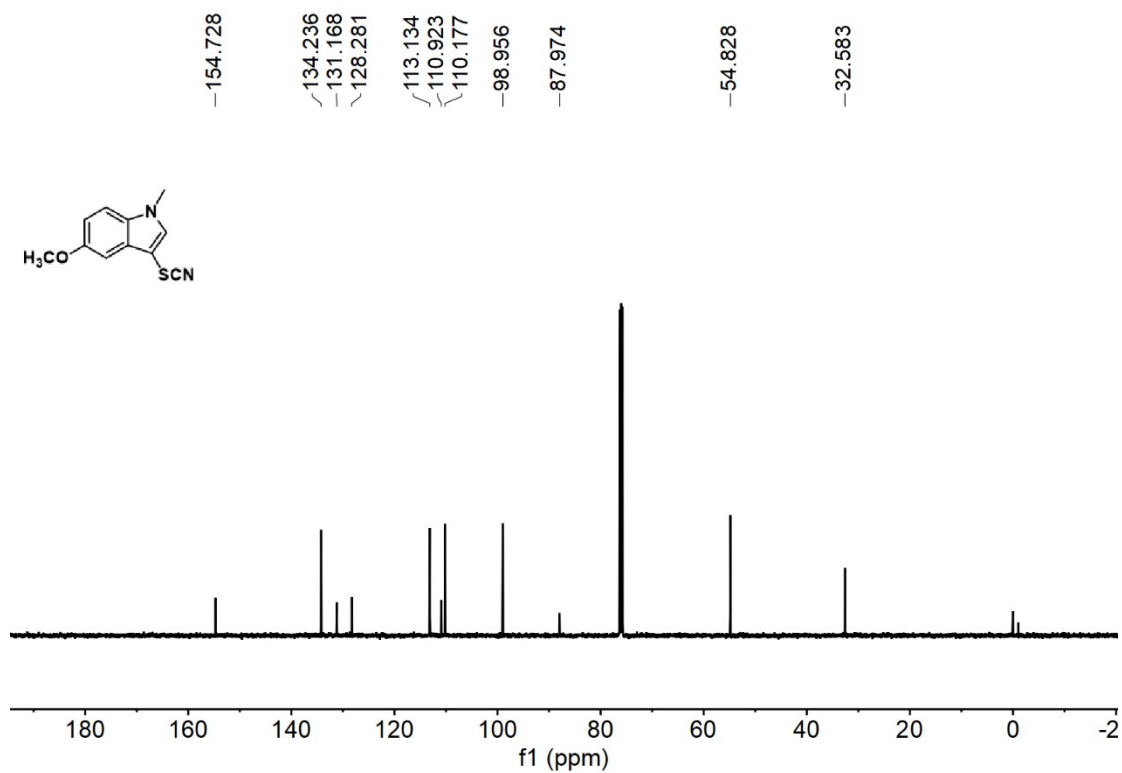


Fig. S24. ¹³C NMR (126 MHz, Chloroform-*d*, 298 K) spectrum of **2d** in CDCl₃.

¹H and ¹³C Spectra of compound 2e (CDCl₃)

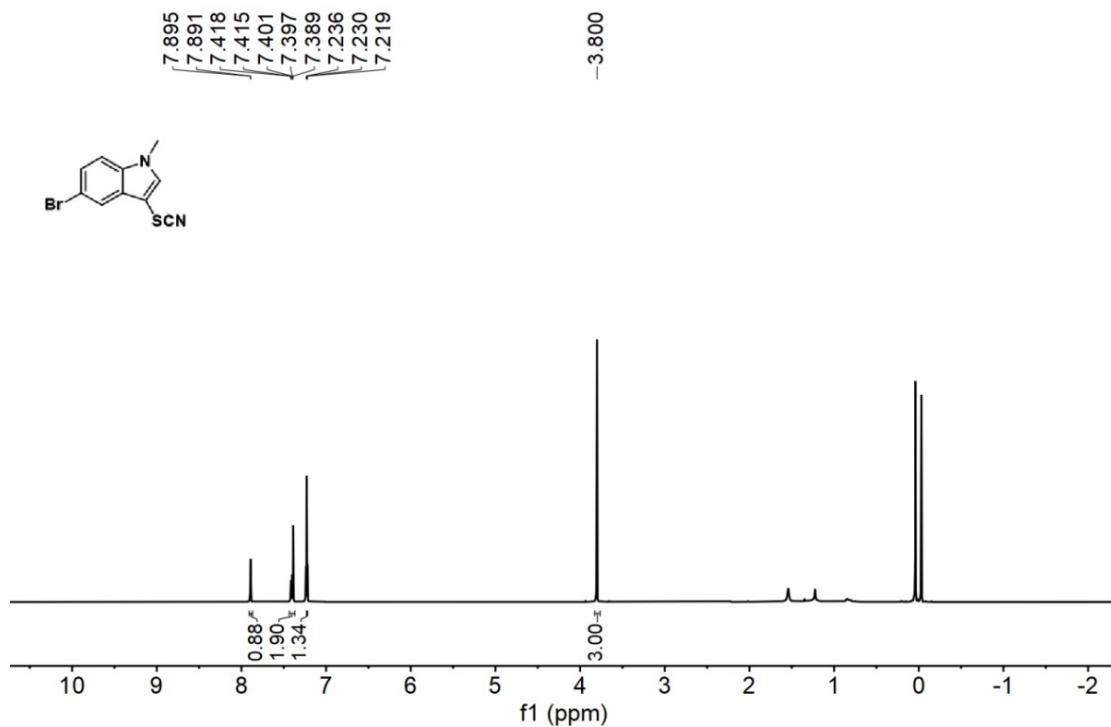


Fig. S25. ¹H NMR (500 MHz, Chloroform-*d*, 298 K) spectrum of **2e** in CDCl₃.

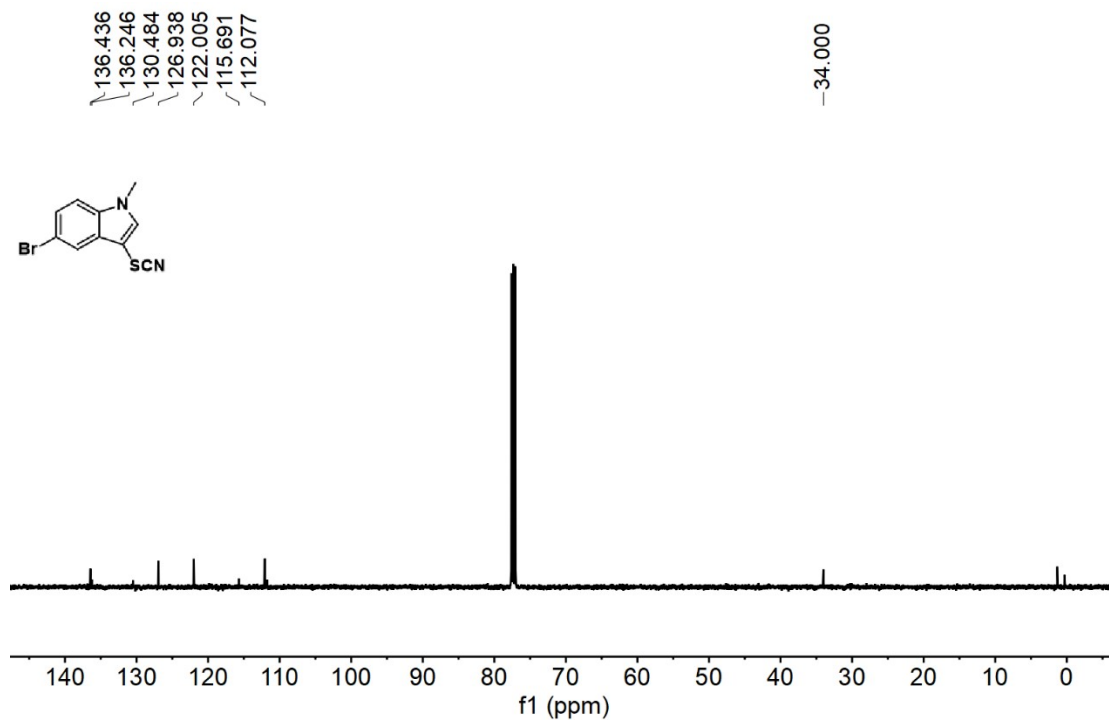


Fig. S26. ¹³C NMR (126 MHz, Chloroform-*d*, 298 K) spectrum of **2e** in CDCl₃.

¹H and ¹³C Spectra of compound 2f (CDCl₃)

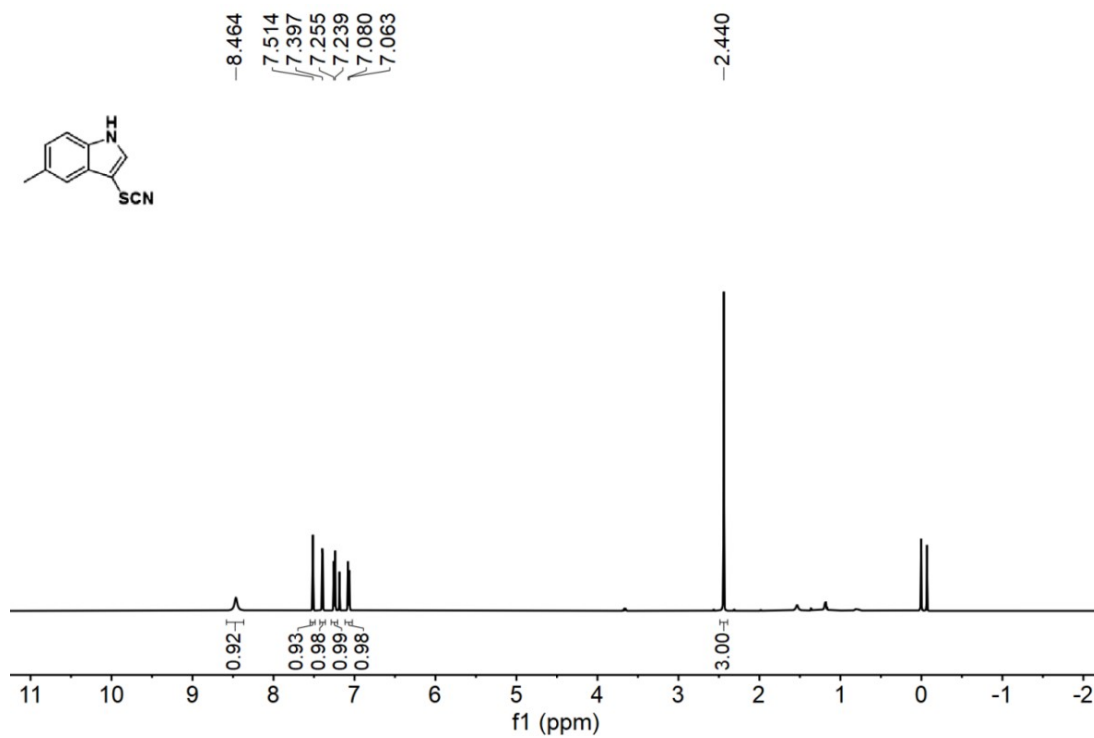


Fig. S27. ¹H NMR (500 MHz, Chloroform-*d*, 298 K) spectrum of **2f** in CDCl₃.

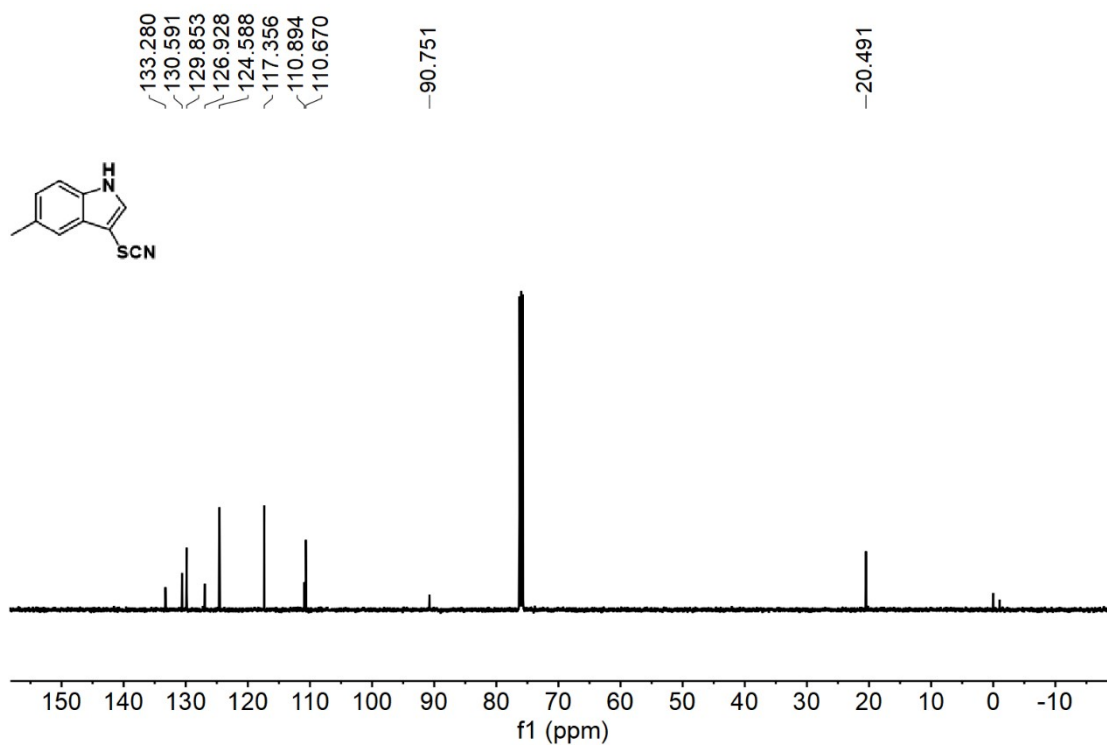


Fig. S28. ¹³C NMR (126 MHz, Chloroform-*d*, 298 K) spectrum of **2f** in CDCl₃.

¹H and ¹³C Spectra of compound 2g (CDCl₃)

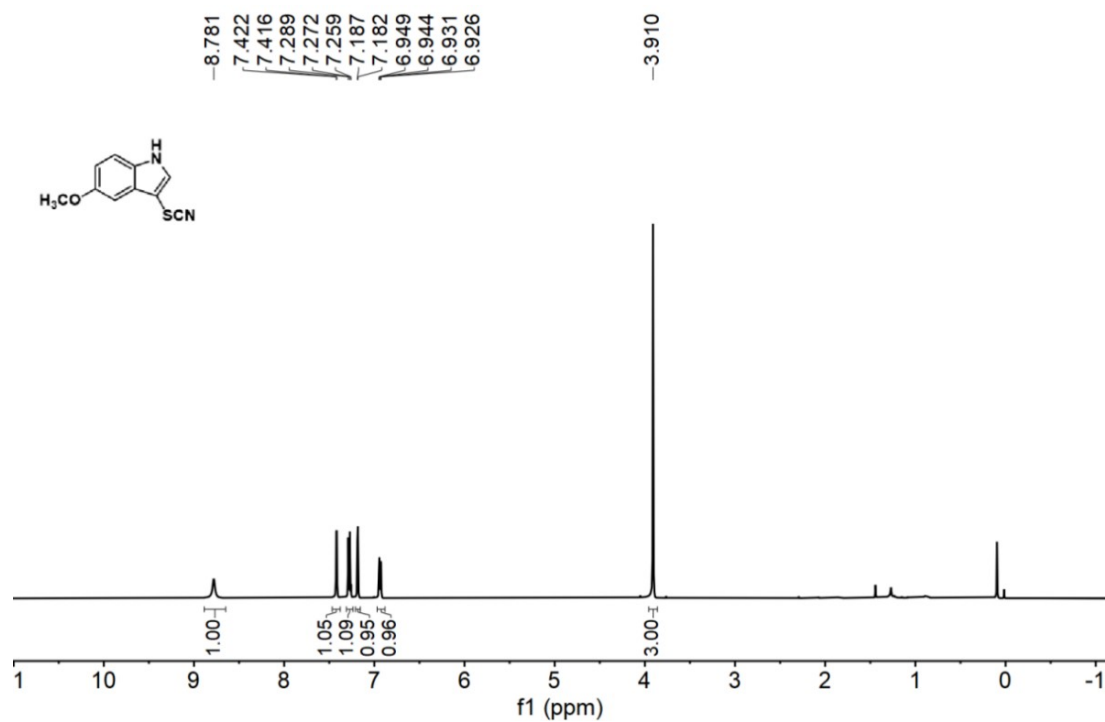


Fig. S29. ¹H NMR (500 MHz, Chloroform-*d*, 298 K) spectrum of **2g** in CDCl₃.

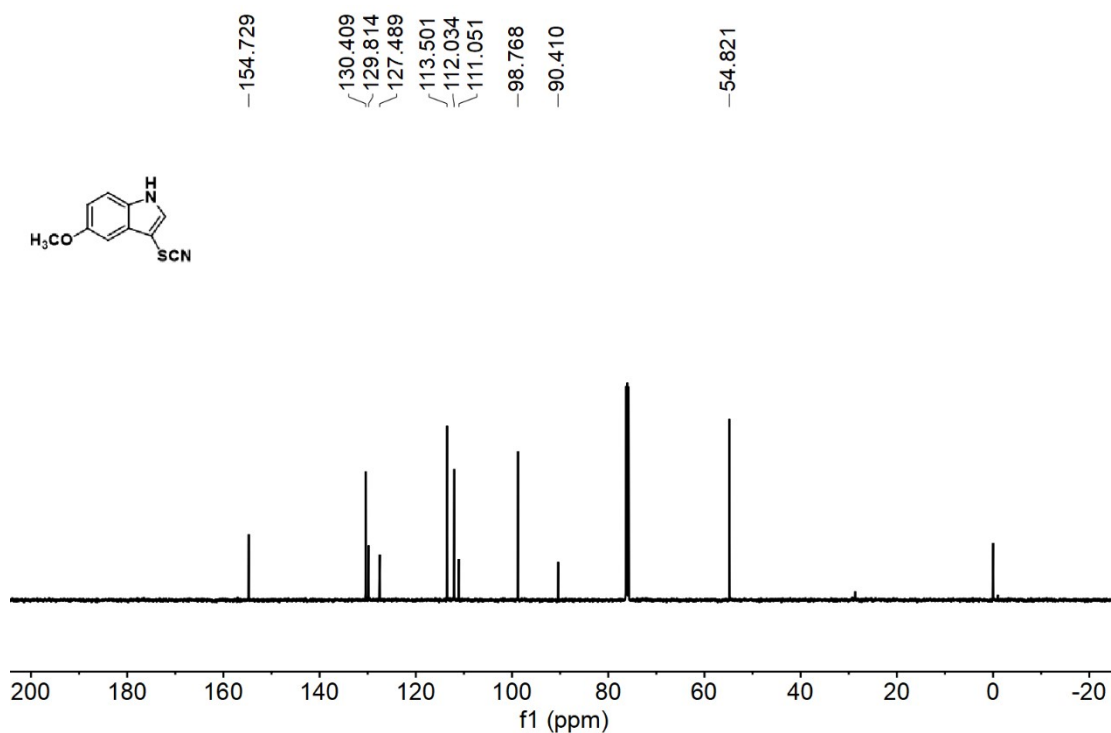


Fig. S30. ¹³C NMR (126 MHz, Chloroform-*d*, 298 K) spectrum of **2g** in CDCl₃.

¹H and ¹³C Spectra of compound 2h (CDCl₃)

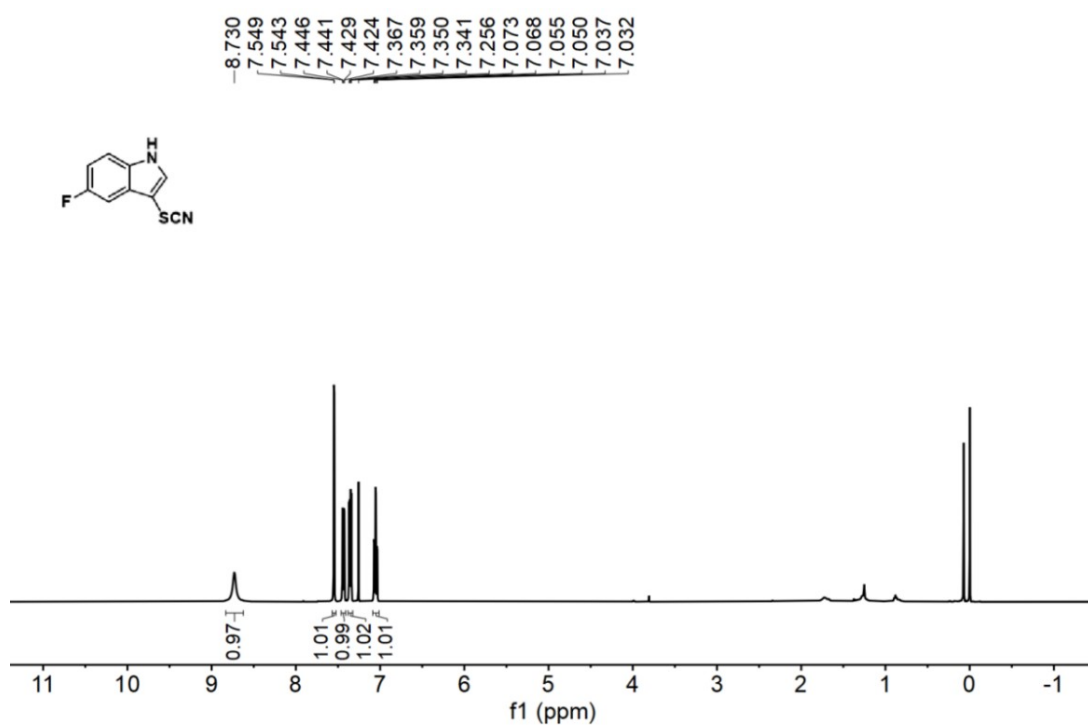


Fig. S31. ¹H NMR (500 MHz, Chloroform-*d*, 298 K) spectrum of **2h** in CDCl₃.

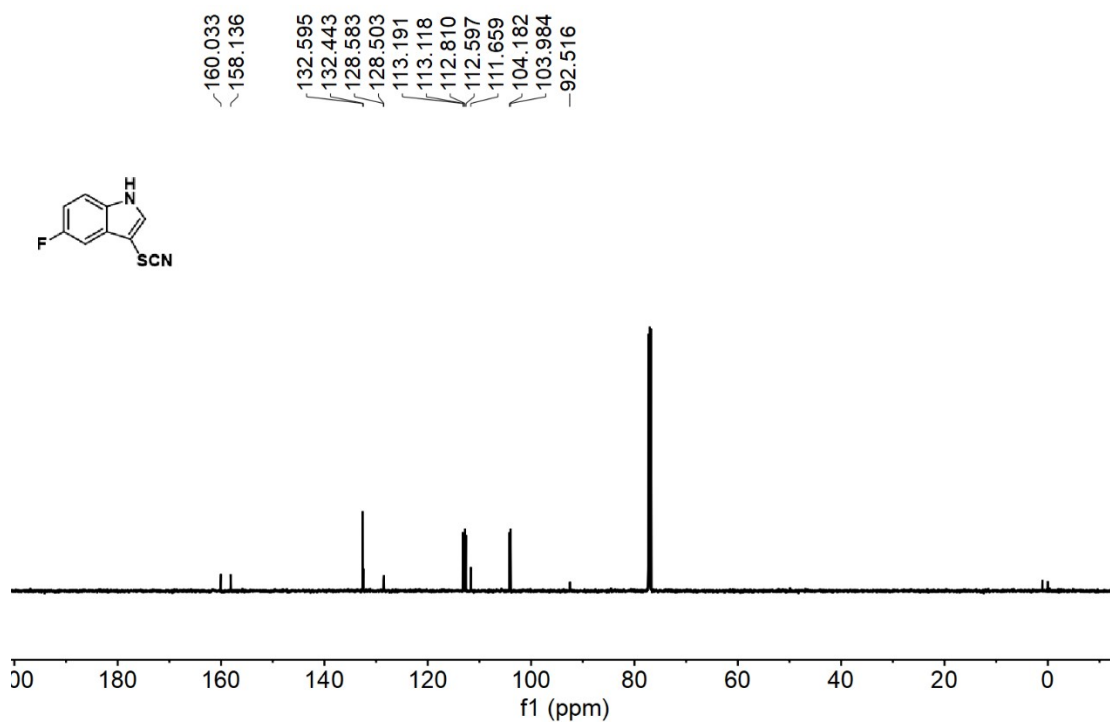


Fig. S32. ¹³C NMR of (126 MHz, Chloroform-*d*, 298 K) spectrum of **2h** in CDCl₃.

¹H and ¹³C Spectra of compound 2i (CDCl₃)

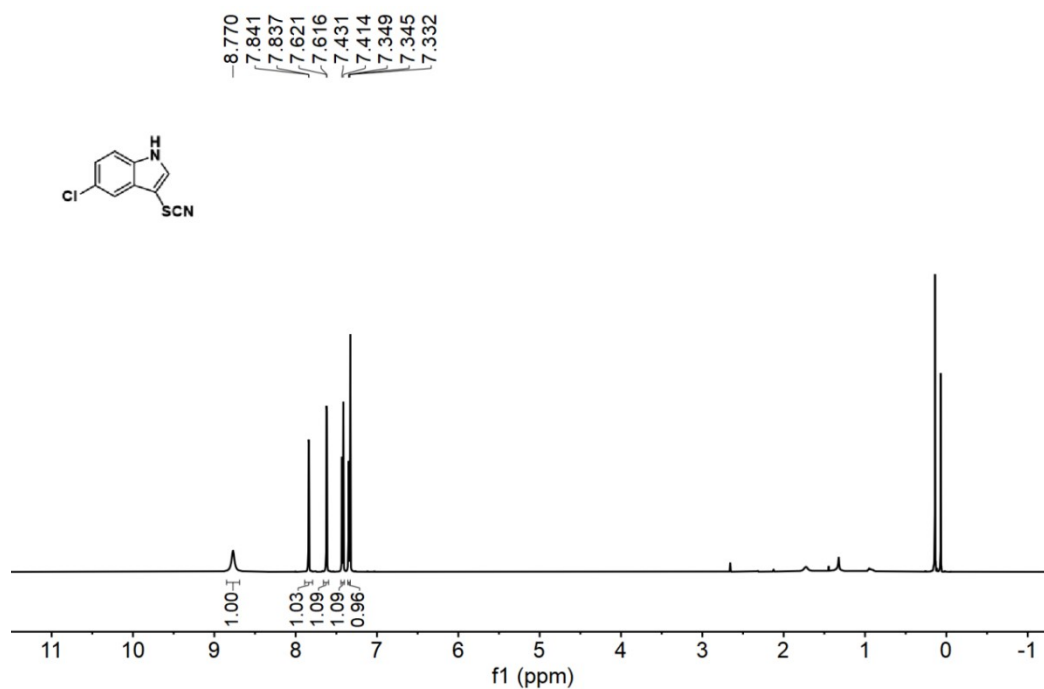


Fig. S33. ¹H NMR (500 MHz, Chloroform-*d*, 298 K) spectrum of **2i** in CDCl₃.

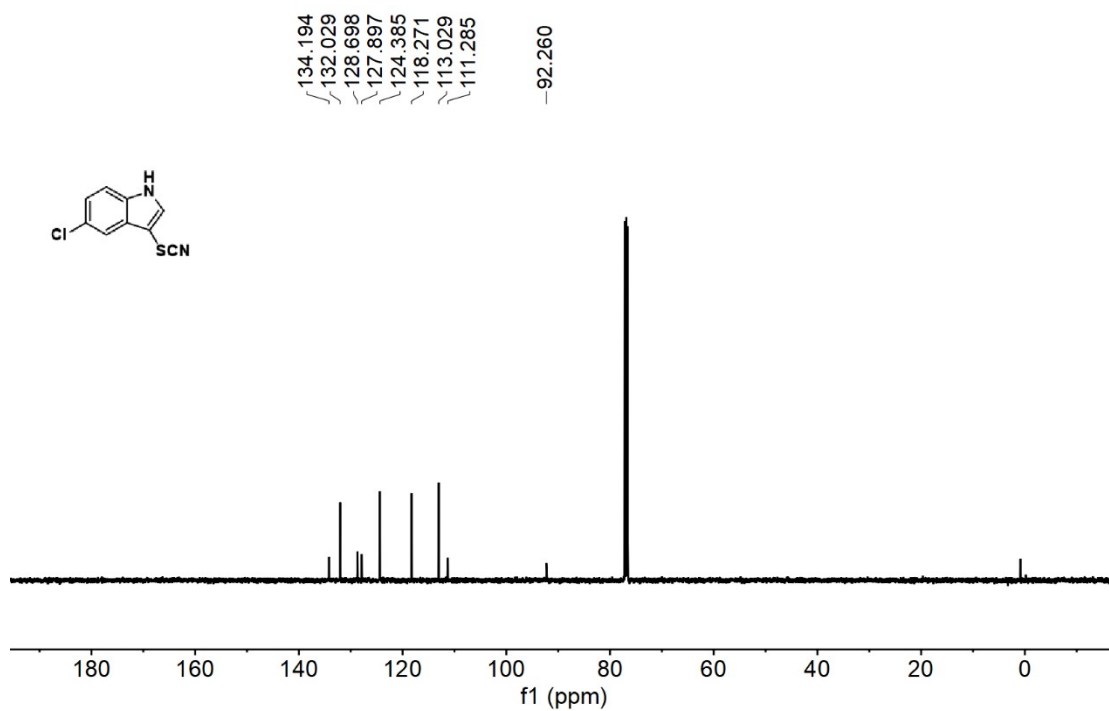


Fig. S34. ¹³C NMR (126 MHz, Chloroform-*d*, 298 K) spectrum of **2i** in CDCl₃.

¹H and ¹³C Spectra of compound 2j (CDCl₃)

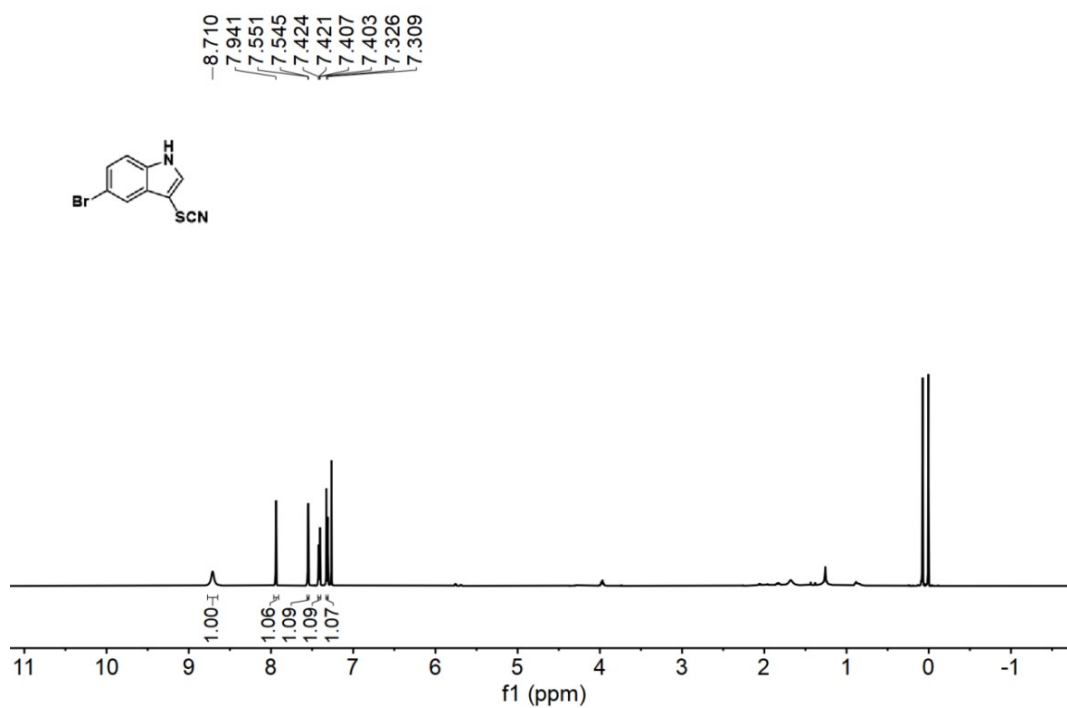


Fig. S35. ¹H NMR (500 MHz, Chloroform-*d*, 298 K) spectrum of **2j** in CDCl₃.

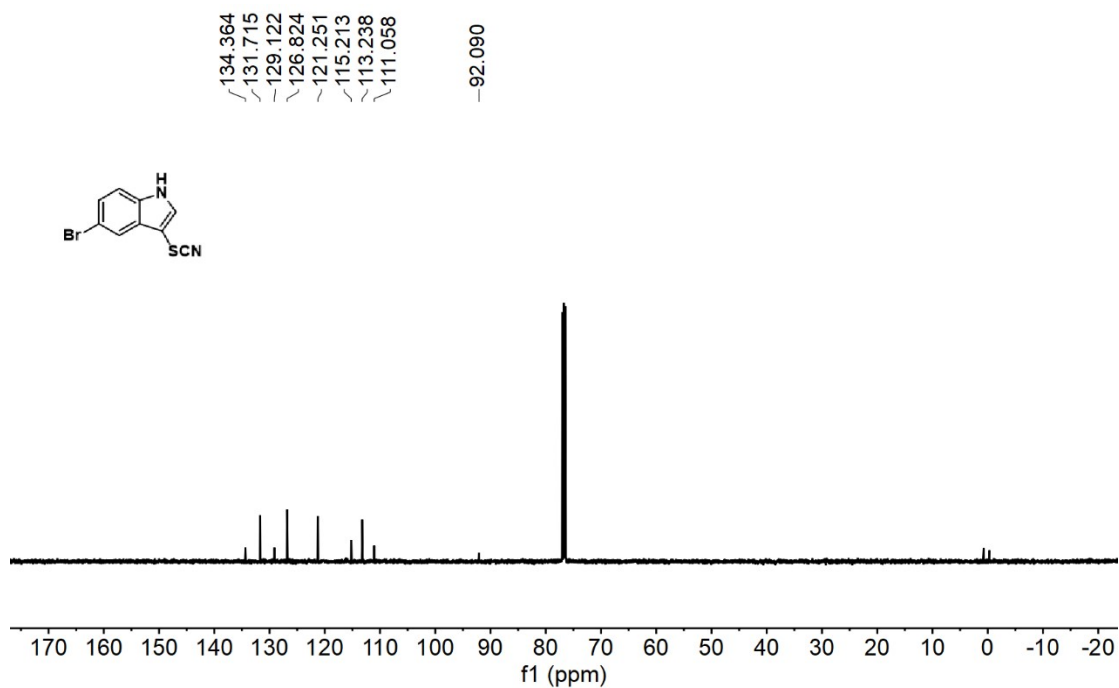


Fig. S36. ¹³C NMR (126 MHz, Chloroform-*d*, 298 K) spectrum of **2j** in CDCl₃.

¹H and ¹³C Spectra of compound 2k (CDCl₃)

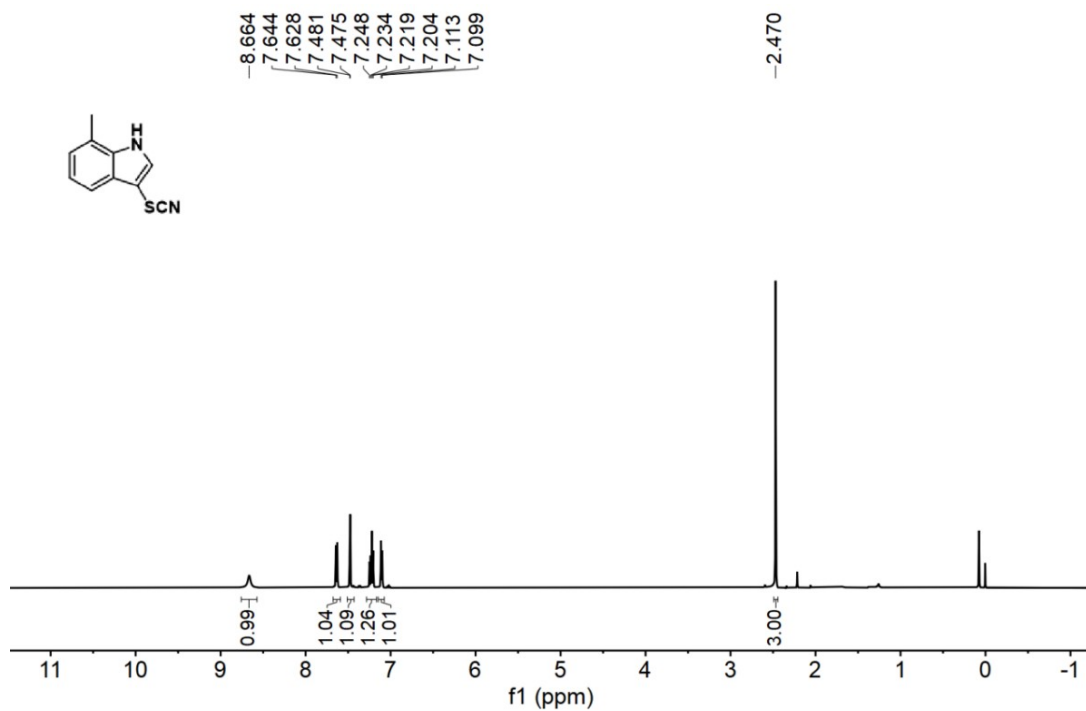


Fig. S37. ¹H NMR (500 MHz, Chloroform-*d*, 298 K) spectrum of **2k** in CDCl₃.

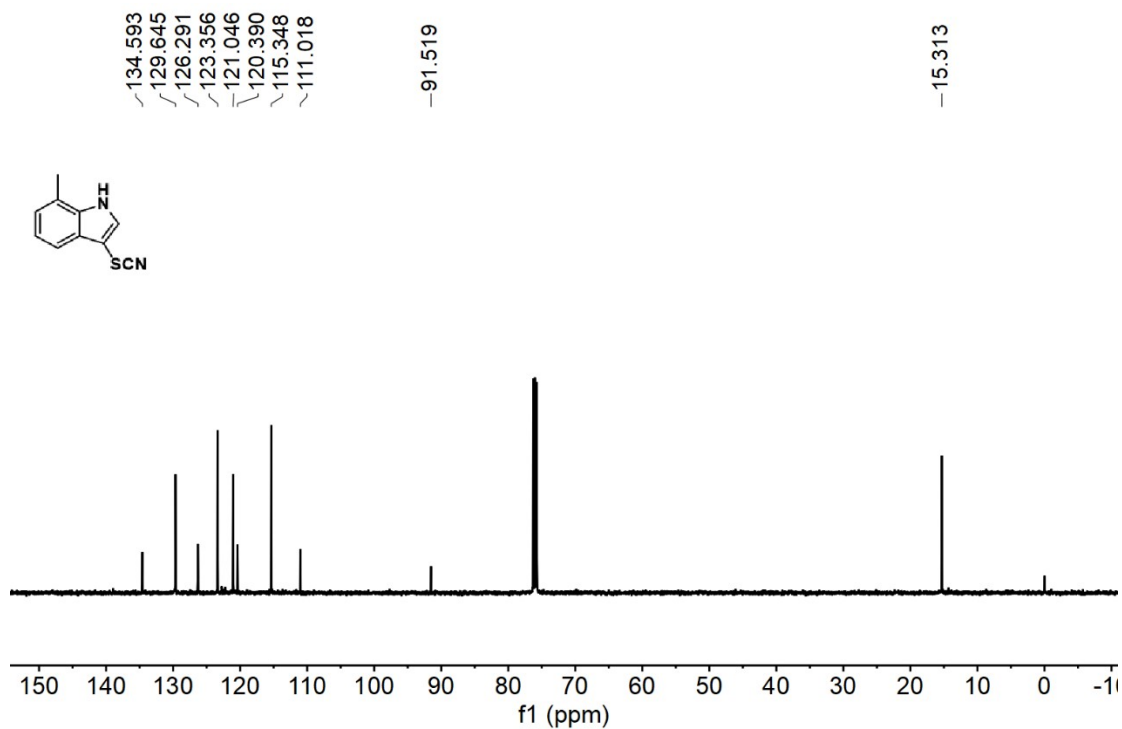


Fig. S38. ¹³C NMR (126 MHz, Chloroform-*d*, 298 K) spectrum of **2k** in CDCl₃.

¹H and ¹³C Spectra of compound 2l (CDCl₃)

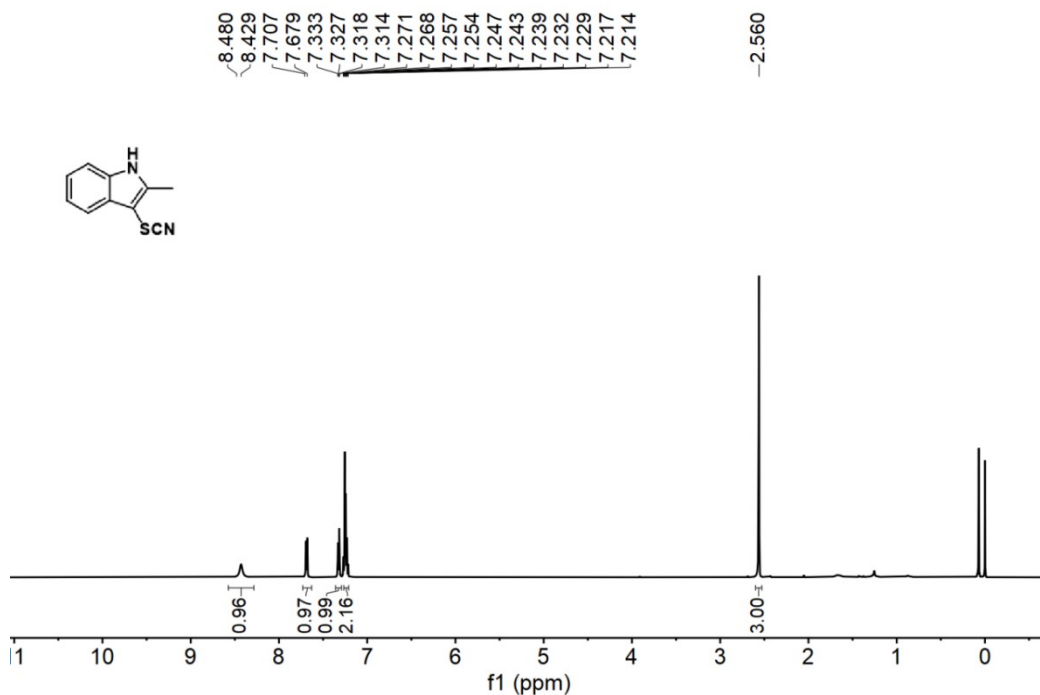


Fig. S39. ¹H NMR (500 MHz, Chloroform-*d*, 298 K) spectrum of **2l** in CDCl₃.

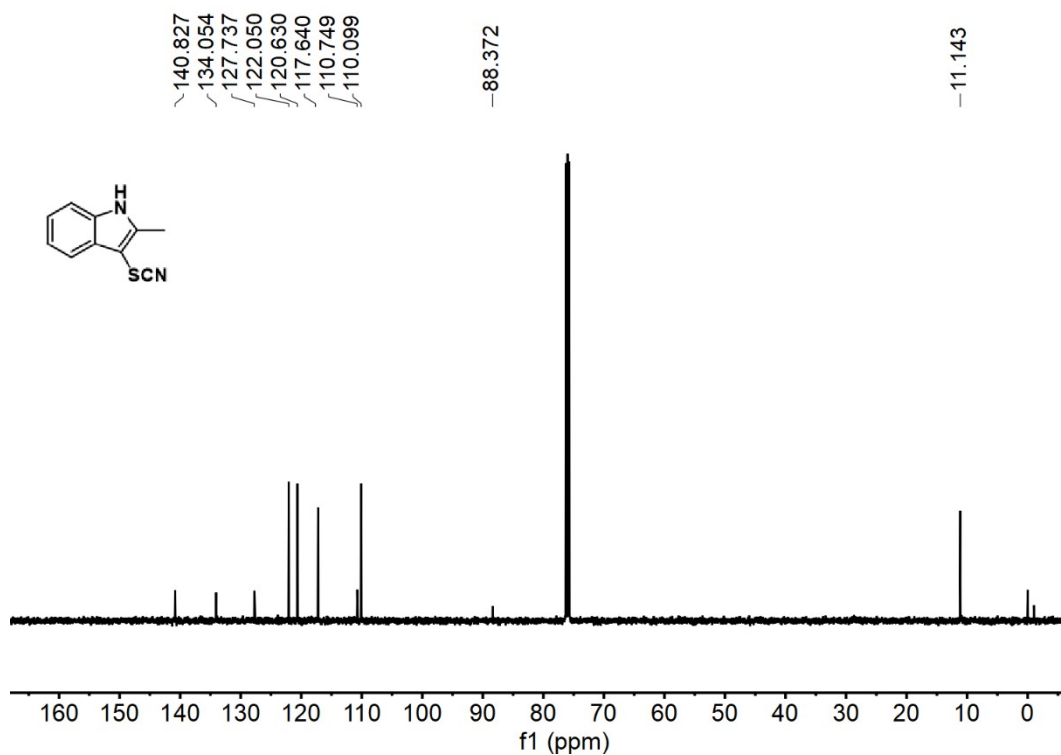


Fig. S40. ¹³C NMR (126 MHz, Chloroform-*d*, 298 K) spectrum of **2l** in CDCl₃.

¹H and ¹³C Spectra of compound 2m (CDCl₃)

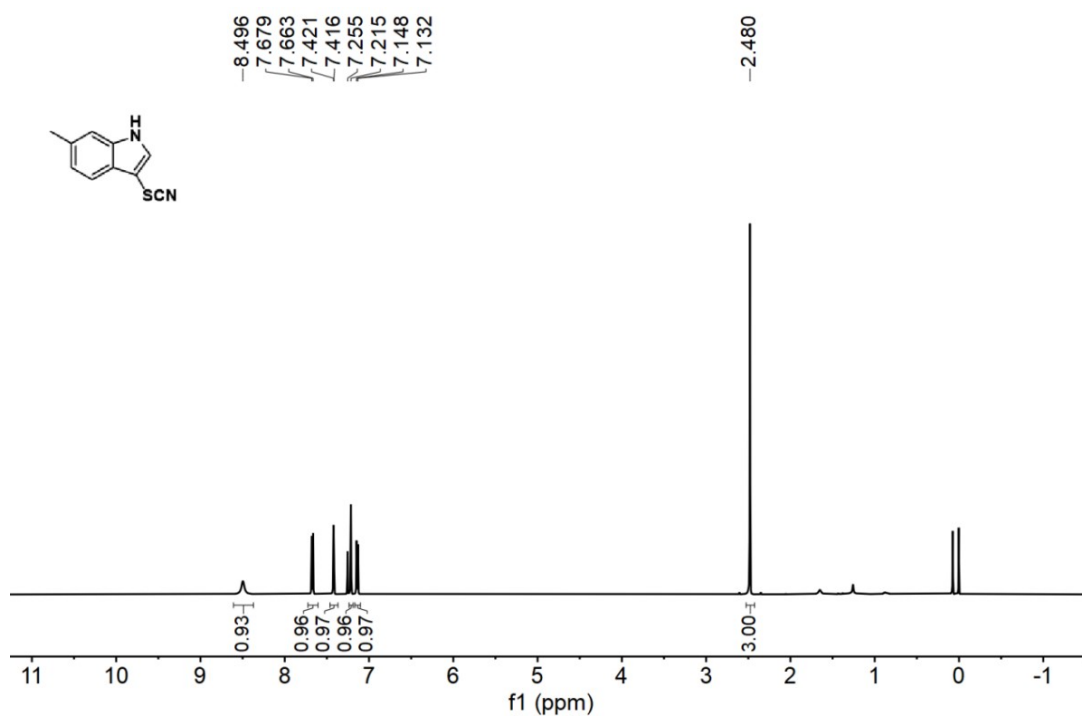


Fig. S41. ¹H NMR (500 MHz, Chloroform-*d*, 298 K) spectrum of **2m** in CDCl₃.

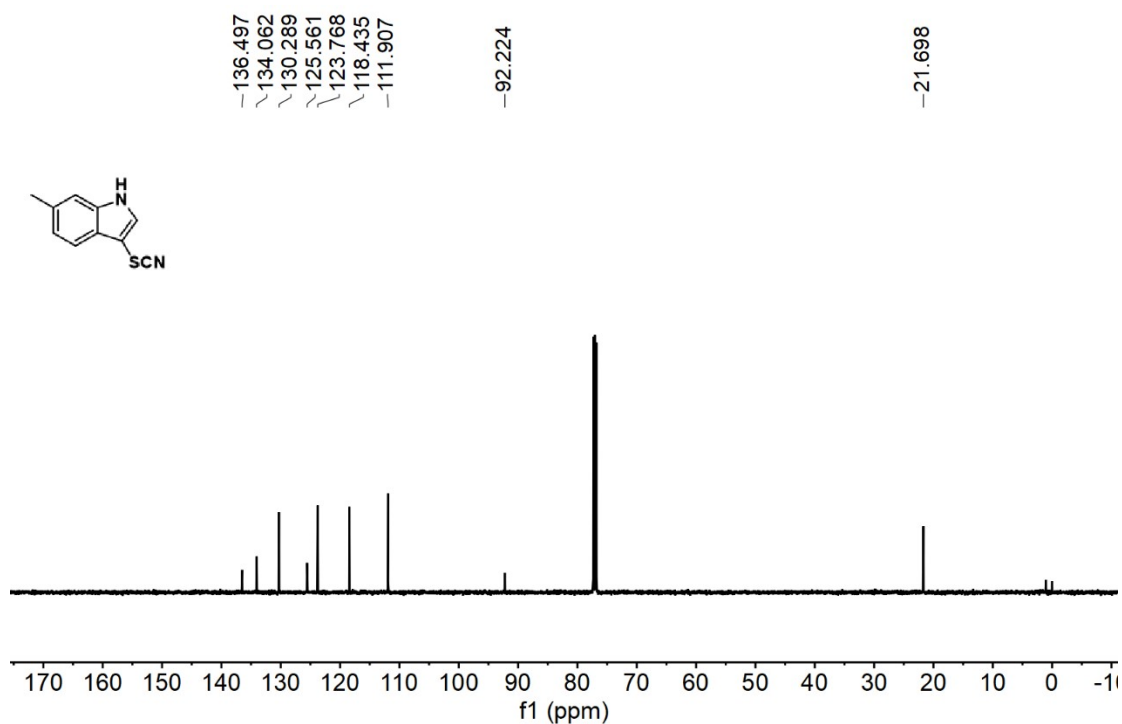


Fig. S42. ¹³C NMR (126 MHz, Chloroform-*d*, 298 K) spectrum of **2m** in CDCl₃.

¹H and ¹³C Spectra of compound 2n (CDCl₃)

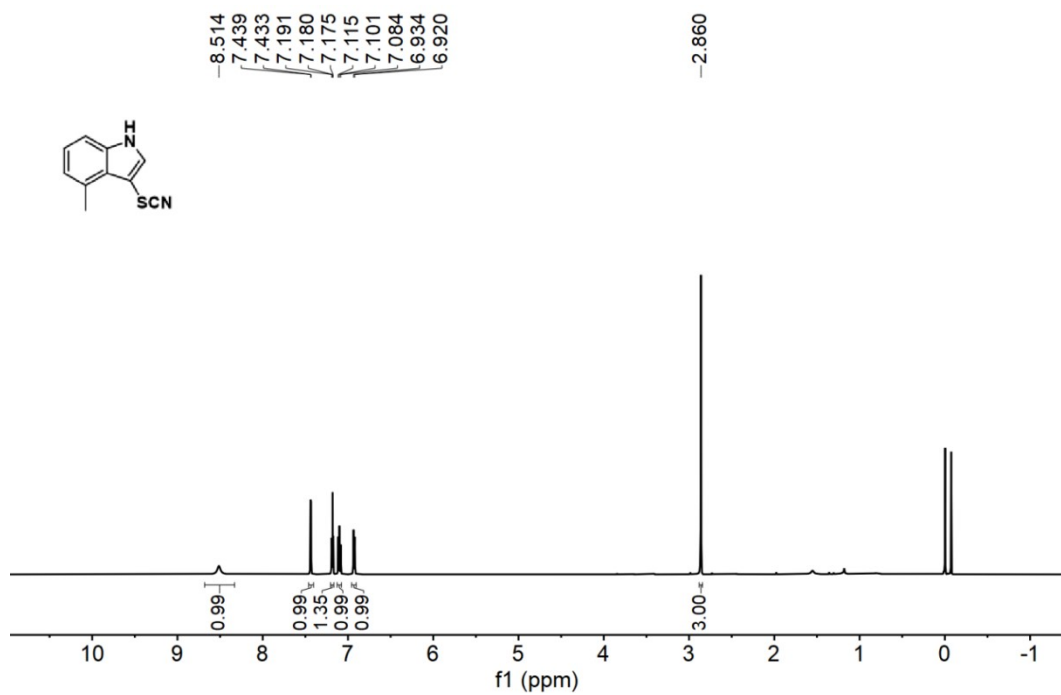


Fig. S43. ¹H NMR (500 MHz, Chloroform-*d*, 298 K) spectrum of **2n** in CDCl₃.

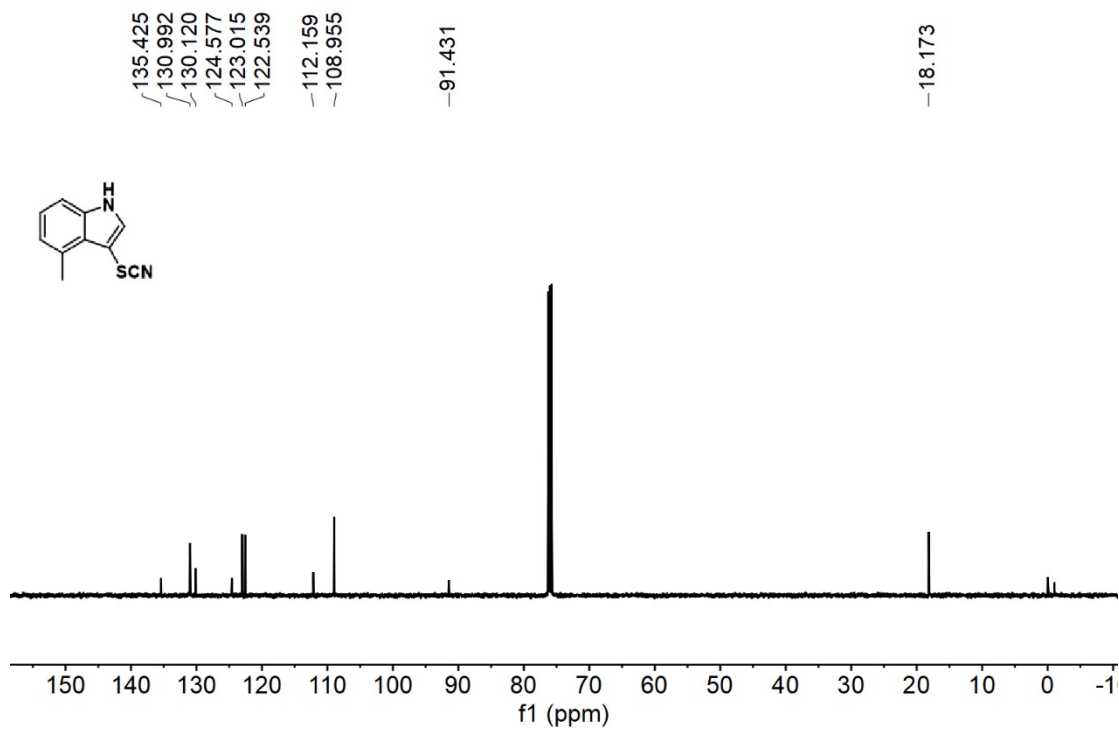


Fig. S44. ¹³C NMR (126 MHz, Chloroform-*d*, 298 K) spectrum of **2n** in CDCl₃.

¹H and ¹³C Spectra of compound 2o (CDCl₃)

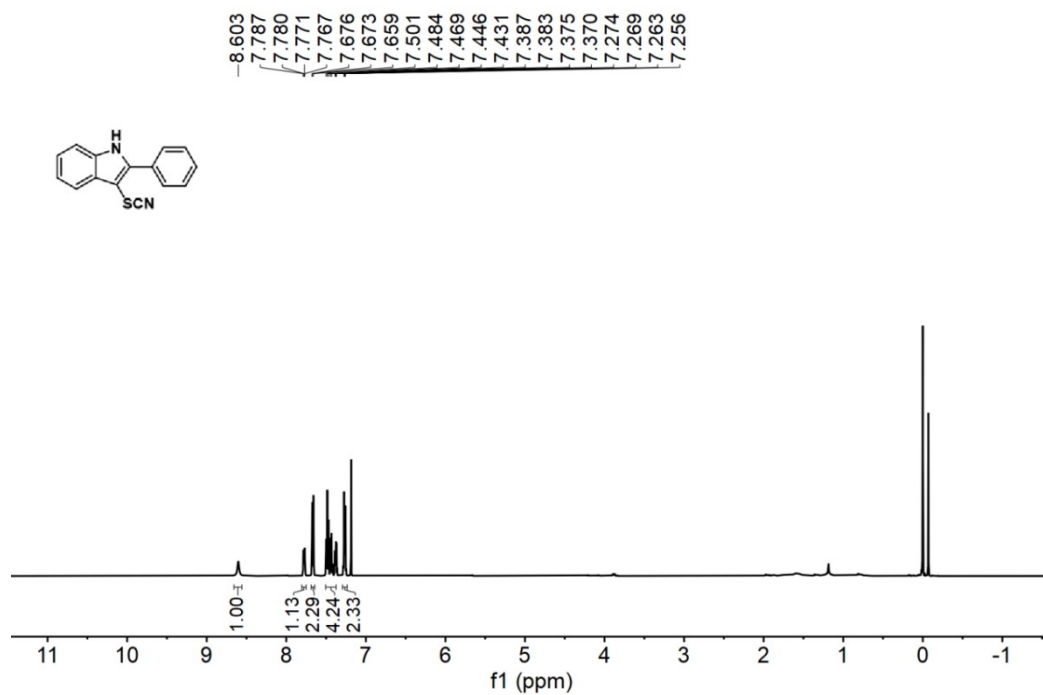


Fig. S45. ¹H NMR (500 MHz, Chloroform-*d*, 298 K) spectrum of **2o** in CDCl₃.

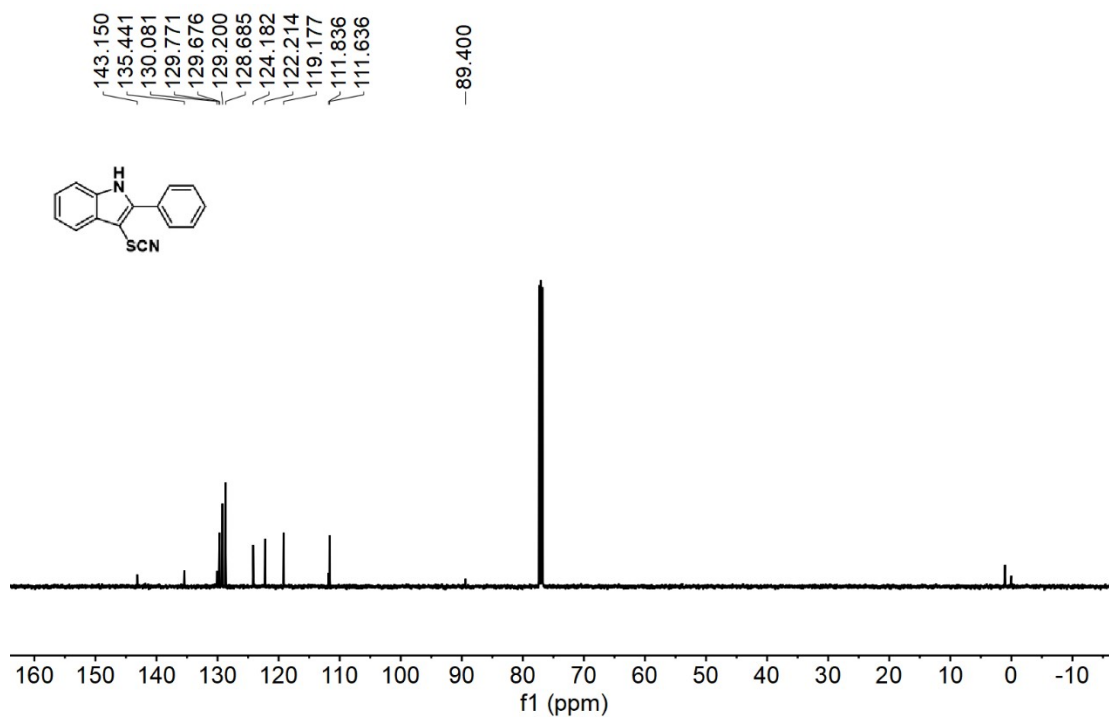


Fig. S46. ¹³C NMR (126 MHz, Chloroform-*d*, 298 K) spectrum of **2o** in CDCl₃.

References

- [1] S. Ma, T. Deng, Z. Li, Z. Zhang, J. Jia, G. Wu, H. Xia, S.-W. Yang and X. Liu, *Angew. Chem. Int. Ed.*, 2022, **134**, e202208919.
- [2] A.C. Uptmoor, F.L. Geyer, F. Rominger and J. Freudenberg, *ChemPlusChem.*, 2018, **83**, 448-454.
- [3] W. Wu, M. Chen, Y. Deng, Q. Tan, Z. Dong, J. Wang, C. Zeng and C. Dai, *Polym. Chem.*, 2023, **14**, 4679-4684.
- [4] Gaussian16, Revision C.01; M.J. Frisch, G.W. Trucks, H.B. Schlegel, G.E. Scuseria, M.A. Robb, J.R. Cheeseman, G. Scalmani, V. Barone, G.A. Petersson, H. Nakatsuji, X. Li, M. Caricato, A.V. Marenich, J. Bloino, B.G. Janesko, R. Gomperts, B. Mennucci, H.P. Hratchian, J.V. Ortiz, A.F. Izmaylov, J.L. Sonnenberg, D. Williams-Young, F. Ding, F. Lipparini, F. Egidi, J. Goings, B. Peng, A. Petrone, T. Henderson, D. Ranasinghe, V.G. Zakrzewski, J. Gao, N. Rega, G. Zheng, W. Liang, M. Hada, M. Ehara, K. Toyota, R. Fukuda, J. Hasegawa, M. Ishida, T. Nakajima, Y. Honda, O. Kitao, H. Nakai, T. Vreven, K. Throssell, J.A. Montgomery, Jr. J.E., Peralta, F. Ogliaro, M.J. Bearpark, J.J. Heyd, E.N. Brothers, K.N. Kudin, V.N. Staroverov, T.A. Keith, R. Kobayashi, J. Normand, K. Raghavachari, A.P. Rendell, J.C. Burant, S.S. Iyengar, J. Tomasi, M. Cossi, J.M. Millam, M. Klene, C. Adamo, R. Cammi, J.W. Ochterski, R.L. Martin, K. Morokuma, O. Farkas, J.B. Foresman, D.J. Fox, Gaussian, Inc., Wallingford CT, 2019.
- [5] A.D. Becke, *Phys. Rev. A*, 1988, **38**, 3098-3100.
- [6] W. Wu, M. Chen, Y. Deng, Q. Tan, Z. Dong, J. Wang, C. Zeng and C. Dai, *Polym. Chem.*, 2023, **14**, 4679-4684.
- [7] K. Cai, W. Wang, J. Zhang, L. Chen, L. Wang, X. Zhu, Z. Yu, Z. Wu and H. Zhou, *J. Mater. Chem. A*, 2022, **10**, 7165-7172.
- [8] M. Hosseini-Sarvari and A.M. Sarvestani, *Photochem. Photobiol. Sci.*, 2021, **20**, 903-911.
- [9] F. Tao, W. Zhou, Z. Li, X. Jiang, L. Wang, Z. Yu, J. Zhang and H. Zhou, *ACS Mater. Lett.*, 2024, **6**, 1120-1129.
- [10] M. Koohgard, Z. Hosseinpour, A.M. Sarvestani and M. Hosseini-Sarvari, *Catal. Sci. Technol.*, 2020, **10**, 1401-1407.

- [11] Z. Li, S. Han, C. Li, P. Shao, H. Xia, H. Li, X. Chen, X. Feng and X. Liu, *J. Mater. Chem. A*, 2020, **8**, 8706-8715.
- [12] W. Fan, Q. Yang, F. Xu and P.-A. Li, *J. Org. Chem.*, 2014, **79**, 10588-10592.
- [13] J. Zhang, F. Tao, W. Wang, C. Gong, Z. Li, W. Zhou, Y. Peng and H. Zhou, *ACS Mater. Lett.*, 2023, **5**, 2799-2806.
- [14] Z. Deng, H. Zhao, X. Cao, S. Xiong, G. Li, J. Deng, H. Yang, W. Zhang and Q. Liu, *ACS Appl. Mater. Interfaces*, 2022, **14**, 35745-35754.
- [15] W. Zhang, J. Tang, W. Yu, Q. Huang, Y. Fu, G. Kuang, C. Pan and G. Yu, *ACS Catal.*, 2018, **8**, 8084-8091.
- [16] T. Zhong, H. Zhu, Y. Zheng, G. Ren, X. Xie, Q. Fan, Z. Xie and Z. Le, *Chem. Commun.*, 2024, **60**, 4230-4233.
- [17] W.-K. An, X. Xu, S.-J. Zheng, Y.-N. Du, J. Ouyang, L.-X. Xie, Y.-L. Ren, M. He, C.-L. Fan, Z. Pan and Y.-H. Li, *ACS Catal.*, 2023, **13**, 9845-9856.
- [18] X. Li, J. Zhou, W. Yin, B. Xie, Z. Liu and J.-J. Liu, *J. Catal.*, 2024, **437**, 115640.
- [19] W. Dai, C. He, S. Li, Y. Xu, F. Cheng and J.-J. Liu, *Inorg. Chem. Front.*, 2024, **11**, 5185-5195.